

Designing asymptotic geodesic hybrid gridshells

Eike Schling^{*a,*}, Hui Wang^{*b}, Sebastian Hoyer^c, Helmut Pottmann^b

^aThe University of Hong Kong, Department of Architecture, Hong Kong

^bKing Abdullah University of Science and Technology, Visual Computing Center, Saudi Arabia

^cTechnical University of Munich, Department of Architecture, Munich

Abstract

Fabrication and assembly of freeform shells can be simplified significantly when controlling the curvature of structural elements during the design phase. This approach has produced fundamental insights to bending-active construction, using the elastic property of elements to form efficient load-bearing structures. This paper is focused on gridshells that are built from straight and flat slats. The slats are combined in two orientations, tangential and normal to the design surface, to create robust and versatile triangulated grids. For this purpose, we generate hybrid webs of asymptotic and geodesic paths on freeform surfaces. The research combines geometric computing with architectural building practice. We present a computational workflow for the design and interactive modification of hybrid asymptotic geodesic webs. At its core are discrete models that are based on concepts of differential geometry and allow to compute constrained structures within an optimization framework. The resulting webs are tested for architectural applications. We derive a strategy for the elastic erection process, in which geodesic lamellas are used as a guide and bracing of the spatial structure. Two architectural scenarios, a timber roof and a steel facade are presented. Their feasibility for construction is verified through prototypical joints and physical models. The research introduces a new class of networks and related surfaces and offers insights into the practical challenges of freeform construction from elastic slats.

Keywords: mesh optimization, asymptotic curves, geodesic curves, construction-aware design, elastic gridshells

1. Introduction

Computational tools allow to embed parameters of fabrication and construction in the design process. This has proven a powerful strategy to design freeform shell structures [1]. Their double curvature offers high structural efficiency with minimal use of material [2], but at the same time creates a high geometric complexity of beams, joints and panels [3]. By implementing geometric constraints, these curved elements can be simplified significantly, creating new possibilities for construction-aware design [4, 5].

One strategy to simplify the fabrication of doubly curved structures is to deform elements into the design shape while maintaining their structural integrity. This strategy has been used in practice to construct elastic gridshells, in which straight elastic rods are assembled on the ground into a flat grid, and then pushed upward and fixed with supports and diagonal bracing to form a highly efficient doubly curved gridshell [6]. This concept has further been developed for thinner and wider slats. The slender laths are less likely to break when twisted and bent around their weak axis, but allow for their strong axis to remain straight and carry external loads.

There is beautiful accordance between the bending of elastic rods in a gridshell and the curvature of curves on a surface in the field of differential geometry [7]. This computational problem becomes more constrained when restricting one axis of curvature. In geometric terms, such lamella grids can be divided into *geodesic networks* (see Fig. 1), exhibiting no geodesic curvature, and *asymptotic networks* (Fig. 2) with vanishing normal curvature. Both networks offer distinct and partly contrary geometric and structural properties, but yield a large range of design solutions.

*Joint first authors contributed equally to this paper

*Corresponding author

Email addresses: schling@hku.hk (Eike Schling*), hui.wang.1@kaust.edu.sa (Hui Wang*), sebastian.hoyer@tum.de (Sebastian Hoyer), helmut.pottmann@kaust.edu.sa (Helmut Pottmann)



Figure 1: Timber Gridshells using geodesic planks. (A) The ribbed Gridshell in Bad Dürrenheim was built with a primary grid along the principal curvature lines and a diagonal cover of geodesic planks. (B) The Expo Hannover Gridshell (by Natterer & Herzog) combines laminated geodesic ribs with a diagonal geodesic substructure. (C) The deployable geodesic Almond Gridshell (by Soriano) was designed to allow a flat assembly and kinetic erection process.



Figure 2: Gridshells using asymptotic networks. (A,B) The first asymptotic timber prototype was developed at the TUM in 2016, using double lamellas of laminated poplar and square timber studs. (C,D) In 2017, the Inside/Out Pavilion was built out of stainless steel lamellas, with repetitive 90-degree joints, and was braced with diagonal pre-stressed cables.

We are looking at the *combination of both geodesic and asymptotic curves*, to design triangulated doubly curved gridshells from exclusively straight and flat slats. Such asymptotic and geodesic (AG) webs profit from a reciprocal stiffness of lying (tangential) and standing (normal) lamellas that are woven together to create a rigid triangular grid. While the asymptotic lamellas offer high structural resilience against normal loads, the geodesic slats offer in-plane stiffness and can be used as the substructure for developable panels.

1.1. Prior work in geometry and geometric computing

Basic ideas underlying the present research have already been outlined by Finsterwalder at the end of the 19th century [8]. In his essay on the mechanical relationships of surface deformation, Finsterwalder describes the geometric properties of geodesic webs as well as asymptotic networks, and their impact on the design freedom of surfaces. This paper is an early and influential contribution towards discrete differential geometry and also contains a wealth of ideas that are now highly relevant for research in computational design and fabrication.

Geometry of webs. From a geometric perspective, the core topic of the present paper are webs of special surface curves, in particular geodesic or asymptotic curves. For the geometry of webs in general, we refer to the monograph by Blaschke and Bol [9]. We are mostly interested in *triangular webs* (called hexagonal in the geometry literature on webs). These consist of three families of curves on a surface, topologically equivalent to part of a regular triangular mesh in the plane. More precisely, there is a parameterization $\mathbf{x}(u, v)$, where the three families of web curves are described by constant u , constant v and constant $u + v$, respectively. We also address *quadrilateral webs* which also

35 contain the curves to constant $u - v$. To fix the notation, we call two families of curves a *curve net*, if there is a regular parameterization where these curves are the parameter lines $u = \text{const}$ and $v = \text{const}$.

In geometry, these curve families are considered as dense, but also discrete webs have been studied. There, one only picks iso-lines of $u, v, u + v$ (possibly also $u - v$), which are integer values. These structures are the most interesting ones for our application.

40 While we are not aware of research on webs containing asymptotic curves, there are results on webs of geodesics. In the plane, these are webs of straight lines. Graf and Sauer [10] have shown that a triangular web of straight lines in the plane is formed by the tangents of an algebraic curve of class 3. The simplest is the obvious case formed by three pencils of parallel lines. There are also studies of triangular webs of geodesics on surfaces. R. Sauer [11] studied them with a discrete model, very much in the spirit of our computational approach to webs, but ours also contain asymptotic
45 curves. He also presented explicit examples on rotational surfaces, which are not just the trivial rotational symmetric arrangements, and examples on spiral surfaces. The characterizing partial differential equation for geodesic webs is found in [12], but its explicit solution appears to be difficult. Clearly, geodesic webs exist on all surfaces of constant Gaussian curvature, since these surfaces can be mapped to the plane so that all their geodesics get mapped to straight lines [10, 13].

50 We will also encounter a relation of our work to conjugate nets of geodesics, studied first by A. Voss [14]. These Voss nets are reciprocal parallel to asymptotic nets on surfaces of constant Gaussian curvature [15]. They possess elegant and remarkable discrete models in form of quad meshes with planar faces that are mechanisms with rigid faces and hinges in the edges [15, 16, 17]. Let us also mention here orthogonal nets of geodesics, which in the smooth setting characterize developable surfaces. Recently, Rabinovich et al. [18, 19] demonstrated the use of discrete models of such
55 nets for geometric design with developable surfaces.

Computational design and fabrication. Computational design of webs formed by geodesics and/or planar curves has been the topic of contributions by Pottmann et al. [20] and Deng et al. [21]. Geodesic webs also appear in form of weaving patterns that generalize the traditional craft of basket weaving to more complex freeform shapes [22, 23, 24]. Working with initially straight ribbons limits the shape space, and thus recent work extended this weaving technique to
60 curved ribbons [25, 26].

We also mention research on grids of elastic rods that form deployable structures. There, an initially flat arrangement can be turned into a curved shape. Motivated by research of Soriano et al. [27], Pillwein et al. [28, 29] compute and design elastic geodesic gridshells, formed by an originally flat arrangements of straight planks. They even provide solutions to the inverse problem of approximating a given shape with such a structure. A similar principle is pursued by
65 the X-shells of Panetta et al. [30], which are not confined to straight rods in the planar state. These structures are more general than the elastic geodesic gridshells, but apparently so far this increased flexibility has not led to a solution of the inverse problem.

Finally, we address the evolution of the present research within architectural geometry and its impact on geometric research. Support structures from single-curved strip-like elements have been addressed by Tang et al. [31]. The
70 practically more interesting case of structures from originally straight lamellas, as provided by asymptotic gridshells, has been the topic of a geometric and computational study by Schling et al. [32]. There, the use of flat circular lamellas of constant radius has already been addressed. It gave rise to a systematic study of so-called principal symmetric meshes, a new type of discrete surface parameterizations [33]. Asymptotic gridshells with a constant node angle represent models of negatively curved surfaces with a constant ratio of principal curvature (CRPC surfaces). They motivated
75 research on CRPC surfaces, especially discrete models [34, 35], where remarkably certain principal symmetric meshes have been the key to represent those with positive Gaussian curvature.

1.2. Architectural precedences

These insights in geometry and computing have had influence on architectural design and construction. There are three specific curvature networks, principal curvature lines, geodesic curves and asymptotic curves, which omit
80 a curvature or torsion (see section 2) and thus allow to simplify the fabrication of elements, beams or panels. *Principal curvature lines* are well suited for doubly curved facade design. A discrete principal curvature mesh offers the use of torsion-free nodes and allows for panelling with planar quadrilateral panels or developable strips [1, 36, 37]). In the Brine Bath in Bad Dürrenheim, the primary structure is designed roughly along the principal curvature paths [38]. Additionally, a layer of densely packed slender slats is used as diagonally bracing, following geodesic curves.

85 Even though the two curvature paths are used independently and don't create a continuous web, this example shows beautifully the potential to create hybrid networks for both geometric and structural benefits (see Fig. 1(A)).

Geodesic gridshells. Any straight strip of material, that is pushed flat onto a curved surface will naturally follow a geodesic curve [20]. Julius Natterer [39] has taken advantage of this principle to prefabricate glue-laminated ribbed shells, from layers of slender timber slats, like the Hannover Expo Roof (see Fig. 1(B)). The layering is necessary to
90 create higher out-of-plane stiffness against external loads, as a single slat would easily buckle. Another thin and dense layer of diagonal slats is used to brace the quadrilateral grid and support the translucent membrane above [40].

Recently, computational developments have pushed experimental research on deployable geodesic gridshells utilizing the simple stacking of slats, pin connections, and easy elastic deformation (see Fig. 1(C)) [41, 42]. Soriano et al. [27] have created a method to design specific geodesic nets that can be assembled flat and deformed into double
95 curvature .

Asymptotic gridshells. Designing asymptotic grids is less intuitive than geodesics. The curve is generated digitally, using a bespoke solver which step by step traces the direction of zero normal curvature on the design surface [43]. This algorithm has been embedded in the Plugin *Bowerbird* [44, 45] for Rhinoceros3D. The workflow of designing a network is tedious, as each curve can only be initiated by a single starting point, and the user can only control the
100 path by changing the curvature of the design surface. To generate a homogeneous grid, each path has to be positioned individually in correspondence to the principal curvature directions [4].

The architectural research on asymptotic grids is quite recent. The first prototype (see Fig. 2(A)) was constructed in timber in 2016 [32]. The lamellas were assembled on two levels to allow for uninterrupted profiles of 60 x 4 mm poplar plywood. Each lamella was built with two slats to create a concentric connection with square timber studs and increase the lateral stiffness (see Fig. 2(B)). A year later, a steel gridshell with approx. 9 m span was constructed at the
105 Technical University in Munich (see Fig. 2(C)). Similar to the timber prototype, the steel joint was built with double lamellas to allow concentric joints and increase the resistance against buckling. The steel, however, was notched and assembled in a single layer and additionally braced using steel cables (see Fig. 2(D)).



Figure 3: Asymptotic networks as façade and transformable structure. (A,B) The asymptotic building envelope prototype was built in 2020, to investigate the application as facade substructure. (C,D): The kinetic umbrella is a transformable structure using GRP lamellas and was completed in 2021.

This construction method has recently been tested for curtain wall applications [46]. The 2.4 x 2.4 m asymptotic
110 building envelope (see Fig. 3(B)) proposes a slender joint with rubber inlays that improved prefabrication and buckling behaviour. A proof of concept showed how panels can be bent onto the asymptotic structure along the principal curvature directions. While this strategy ensures that all panels are perfectly developable, both panels and flat press-strips do not follow geodesic directions and have to be fabricated with individual geodesic curvature (see Fig. 3(A)).

In contrast to geodesics, most asymptotic gridshells can naturally be assembled flat. The deformation from flat
115 to curved shape occurs along a compliant mechanism, due to scissor joints and restricted bending of lamellas [47]. This makes the erection process easy with no need for additional formwork. Schikore et al.[47] take advantage of this property to design transformable roof structures, and control their kinetic behaviour. The Kinetic Umbrella (see Fig. 3(C)) was constructed in 2021 from single 8 x 80 mm glass-fibre reinforced plastic (GRP) rods connected by eccentric aluminium joints (see Fig. 3(D)). The structure transforms from a 6 m tall cylinder to a wide funnel shape of

120 approx. 8 m diameter.

The constructive development of geodesic and asymptotic structures have produced various solutions in timber, steel and glass-fibre. The dominant mode of failure of these structures is local buckling due to compression, or lateral-torsional buckling due to bending of the slender lamellas [46]. Strategies to tackle this issue focused on layering or coupling of lamellas. So far, the hybrid use of geodesic and asymptotic lamellas to create reciprocal stiffness has not been investigated. Geodesics have further proven valuable not only as structural grid, but also as a means to cover a ribbed shell with parallel straight slats. This potential has not been applied to asymptotic structures. Here, we see a specific potential of creating straight developable panels and straight pressure-strips.

1.3. Overview and contributions

We are interested in combining asymptotic (A, blue) and geodesic (G, red) curves in a structural networks (see Fig. 4). Curves which are asymptotic and geodesic at the same time, must be straight. We do not further study structures containing them, since their shapes are restricted to ruled surfaces. Far more versatile are AG-nets, in which three or four families of curves are combined to meet in the same intersection points. AGG-webs make use of only one asymptotic family and create triangulations by adding two geodesic families. AAG-webs combine two families of asymptotic curves with a single family of geodesics. A 4-web AGAG of two families of asymptotic curves and two families of geodesics offers higher density, but is strongly restricted in its design freedom. These combinations of webs can be extended to partial webs, which allow to extend the design surface into positive curvature for dome-like construction using only geodesic lamellas.

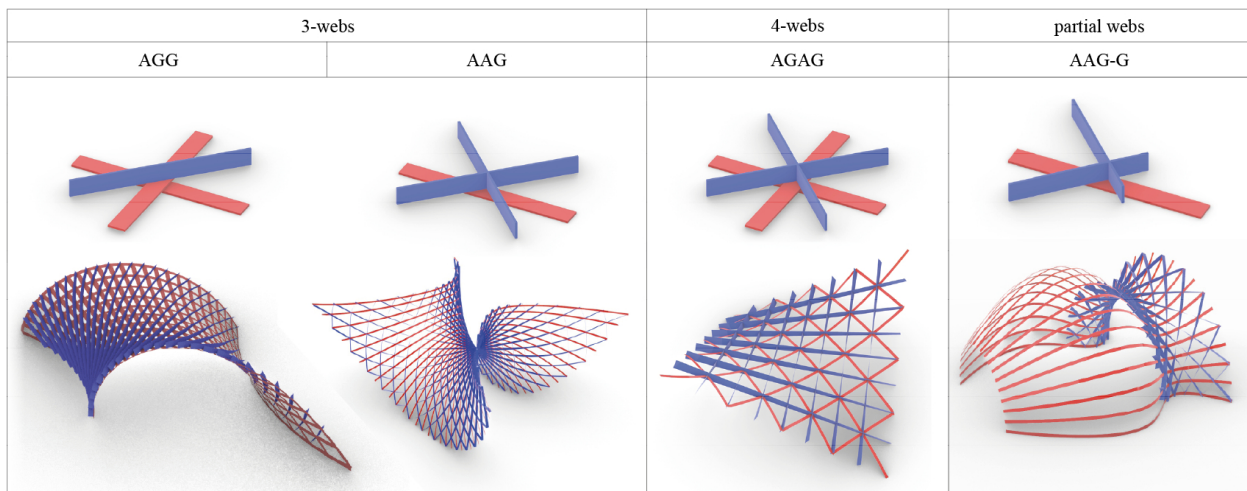


Figure 4: Overview of the possible 3- and 4-webs combining asymptotic (A,blue) and geodesic (G,red) lamellas. Partial webs may extend the geodesic network onto surface regions of positive curvature.

This publication introduces a novel computational method to design asymptotic-geodesic webs, and offers architectural experiments and scenarios for their construction as elastic gridshells.

Section 2 briefly describes the required concepts from differential geometry that are underlying our mathematical model. In particular, we discuss the special webs whose design and fabrication is our main target. Section 3 discusses the discretization of the geometric structures under consideration. This is the basis of the numerical optimization algorithm that forms the core of the computational design tool. We also go beyond a purely discrete model and briefly address how to obtain smooth curved elements. It is used to create the developable strips and unroll them to the plane. Finally, a design workflow is established to link this optimization to Rhino-Grasshopper and allow architects to engage and design with this novel tool using specific controls such as boundary constraints, fairness and proximity. Section 4 presents the architectural implementation for AAG-webs. Physical experiments investigate the assembly and erection process with focus on the positioning and fixing of geodesics. Two architectural scenarios are designed for timber and steel to investigate the constructive benefits of combining tangential and normal lamellas to increase structural stiffness

150 and create smooth facades from developable strips. We discuss the challenges of construction, erection, tolerance and performance. Section 5 concludes our findings in the computational workflow, design and construction and highlights future areas of investigation.

2. Geometric fundamentals

155 In order to make this research accessible for computational designers, architects and engineers, we recall here some basic concepts of elementary differential geometry. This is important to understand the subsequently presented computational approach and its implementation. For more details, see e.g. [48, 49].

2.1. Frenet frame, Darboux frame and curvatures

The *Frenet frame* is an orthonormal frame, attached to a curve \mathbf{c} . Let the curve be given in an arc length parameterization $\mathbf{c}(s)$ and primes denote derivatives with respect to s . Then the Frenet frame is formed by the unit tangent vector $\mathbf{e}_1 = \mathbf{t} = \mathbf{c}'$, the principal normal vector $\mathbf{e}_2 = \mathbf{c}''/\|\mathbf{c}''\|$ and the binormal vector $\mathbf{e}_3 = \mathbf{e}_1 \times \mathbf{e}_2$. Vectors $\mathbf{e}_1, \mathbf{e}_2$ span the *osculating plane* of the curve. The derivatives of the frame vectors with respect to s satisfy the Frenet equations, which may be written in the form

$$\mathbf{e}_i' = \mathbf{d} \times \mathbf{e}_i, \quad i = 1, 2, 3. \quad (1)$$

Here, $\mathbf{d} = \tau \mathbf{e}_1 + \kappa \mathbf{e}_3$ is the angular velocity vector of the frame's motion, also known as Darboux vector for this frame. Its coordinates with respect to the Frenet frame exhibit the *curvature* κ and *torsion* τ of the curve (see Fig. 5).

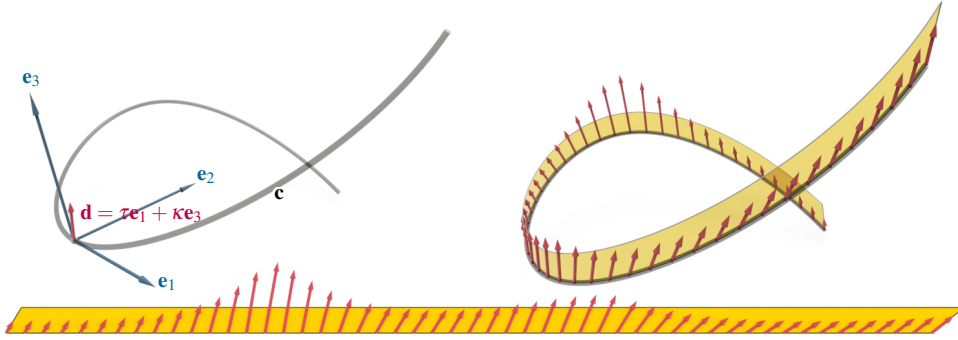


Figure 5: Left: The Darboux vector \mathbf{d} in the rectifying plane of the Frenet frame attached to a space curve \mathbf{c} . Right: The Darboux vectors at all curve points define the rulings of the rectifying developable surface D through \mathbf{c} . Bottom: In the planar development of D , the curve \mathbf{c} lies in a straight line.

Let us now consider a curve $\mathbf{c}(s)$ which lies on a surface S . Then, the *Darboux frame* $(\mathbf{t}(s), \mathbf{u}(s), \mathbf{n}(s))$ of \mathbf{c} with respect to S is formed by the unit tangent vector $\mathbf{t} = \mathbf{e}_1$, unit surface normal vector \mathbf{n} and unit side vector $\mathbf{u} = \mathbf{n} \times \mathbf{t}$ (see Fig. 6). Their derivatives satisfy the equations

$$\mathbf{t}' = \mathbf{r} \times \mathbf{t}, \quad \mathbf{u}' = \mathbf{r} \times \mathbf{u}, \quad \mathbf{n}' = \mathbf{r} \times \mathbf{n}, \quad \text{with } \mathbf{r} = \tau_g \mathbf{t} - \kappa_n \mathbf{u} + \kappa_g \mathbf{n}. \quad (2)$$

160 Now we have denoted the angular velocity vector of the frame motion by \mathbf{r} . It is also called *Darboux vector*, but here with respect to the Darboux frame. Its representation with respect to the Darboux frame exhibits the already encountered invariants of a curve on a surface, namely *geodesic torsion* τ_g , *normal curvature* κ_n and *geodesic curvature* κ_g . Since \mathbf{r} decomposes into rotations about the frame vectors \mathbf{t} , \mathbf{u} , and \mathbf{n} with angular velocities τ_g , $-\kappa_n$ and κ_g , respectively, we have a kinematic interpretation of these quantities by the instantaneous rotations of the Darboux frame about its axes, indicated in Fig. 6.

165 Because of

$$\mathbf{c}'' = \mathbf{t}' = \mathbf{r} \times \mathbf{t} = \kappa_n \mathbf{n} + \kappa_g \mathbf{u},$$

κ_n and κ_g are just the projections of the curvature vector \mathbf{c}'' onto \mathbf{n} and \mathbf{u} , respectively, implying $\kappa^2 = \kappa_g^2 + \kappa_n^2$.

Let us repeat the meaning of vanishing κ_g or κ_n at all points of a curve, since it plays a fundamental role in the present context.

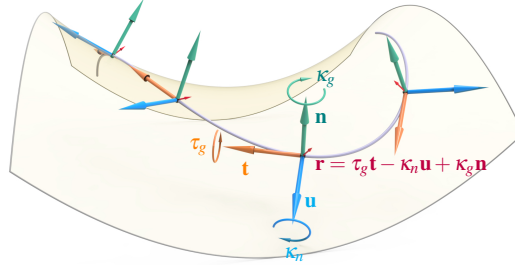


Figure 6: The Darboux frame depicting the three “curvatures” τ_g , κ_n , κ_g of a curve on a surface.

- $\kappa_g = 0$ at all points characterizes a *geodesic curve* c on S . It is, at least locally, a shortest path on S . The curvature vector $\mathbf{c}'' = \kappa_n \mathbf{n}$ of \mathbf{c} is orthogonal to the surface. In other words, the principal normal \mathbf{e}_2 agrees with the surface normal \mathbf{n} ; the osculating plane is orthogonal to the tangent plane. Darboux frame and Frenet frame are rotated against each other by a right angle: $\mathbf{e}_2 = \mathbf{n}$, $\mathbf{e}_3 = -\mathbf{u}$. This implies $\kappa_n = \kappa$ and $\tau_g = \tau$.
- A curve \mathbf{c} with $\kappa_n = 0$ at all points is called an *asymptotic curve*. Each tangent of \mathbf{c} is an asymptotic direction of S , i.e. one with vanishing normal curvature. Asymptotic directions exist only in areas of S where the Gaussian curvature K is not positive. Now we have $\mathbf{c}'' = \kappa_g \mathbf{u}$, so that $\mathbf{e}_2 = \mathbf{u}$ and thus $\mathbf{e}_3 = \mathbf{n}$. Darboux frame and Frenet frame agree, the osculating plane of the asymptotic curve \mathbf{c} agrees with the tangent plane of S . Comparing the expressions of the Darboux vectors \mathbf{d} and \mathbf{r} , we find $\kappa_g = \kappa$ and $\tau_g = \tau$.

Let us remark that normal curvature and geodesic torsion of a curve \mathbf{c} at a surface point $\mathbf{p} \in S$ depend on the angle between the curve tangent \mathbf{t} against the principal curvature directions $\mathbf{t}_1, \mathbf{t}_2$ and on the corresponding principal curvatures κ_1, κ_2 . Recall that $\mathbf{t}_1, \mathbf{t}_2$ are orthogonal tangent directions of S at \mathbf{p} . If ϕ is the angle of \mathbf{t} against \mathbf{t}_1 , we have

$$\kappa_n = \kappa_1 \cos^2 \phi + \kappa_2 \sin^2 \phi, \quad \tau_g = \frac{1}{2}(\kappa_2 - \kappa_1) \sin 2\phi. \quad (3)$$

This shows that κ_1, κ_2 are the normal curvatures to principal directions $\mathbf{t}_1, \mathbf{t}_2$ and the extreme values of κ_n . Moreover, $\kappa_n = 0$ is not possible for $K = \kappa_1 \kappa_2 > 0$. We also see that geodesic torsion vanishes for principal directions, so that a curve with $\tau_g = 0$ at all points is a principal curvature line. Geodesic torsion τ_g attains its extreme values $\pm(\kappa_2 - \kappa_1)/2$ for $\phi = \pm\pi/4$, i.e., the bisecting directions of the principal directions.

Note that geodesic and normal curvature, as well as geodesic torsion are defined for a curve with respect to a surface. If we keep the curve, but change the surface, these values will in general change.

2.2. Bending a straight strip and attaching it to a surface

In the following we have to consider two surfaces, namely the given reference surface S and the surface formed by the bent slat. The latter surface is formed by bending an originally flat strip of material. For the materials and fabrication process underlying our application, it is sufficient to neglect any stretching of the material during deformation, at least for geometric modeling. This means that the deformation is isometric and keeps the length of curves, angles between curves, geodesic curvature of curves and the Gaussian curvature $K = \kappa_1 \kappa_2$ of the surface unchanged. We build our structures from flat slats with straight boundaries. Bending such a strip, one obtains a developable surface strip D ($K = 0$). It has only a one-parameter family of tangent planes, which we study now. The long boundaries and central curve \mathbf{c} are parallel geodesics on D . Hence, at each point $\mathbf{c}(s)$ of \mathbf{c} , the tangent plane $T(s)$ of D is orthogonal to the osculating plane of $\mathbf{c}(s)$. Thus $T(s)$ is the so-called *rectifying plane*, spanned by tangent $\mathbf{e}_1(s)$ and binormal $\mathbf{e}_3(s)$. D is therefore called *rectifying developable* of \mathbf{c} . It is the only developable surface D one can pass through a curve \mathbf{c} so that after unrolling D into the plane the curve becomes a straight line (see Fig. 5).

Each tangent plane $T(s)$ of the rectifying developable D touches D along a straight line, called a *ruling*. It can be computed by intersecting $T(s) : (\mathbf{x} - \mathbf{c}(s)) \cdot \mathbf{e}_2(s) = 0$ with the derivative plane $T'(s) : (\mathbf{x} - \mathbf{c}(s)) \cdot \mathbf{e}'_2(s) = 0$. The resulting ruling $R(s)$ has direction vector $\mathbf{r}_D = \mathbf{e}_2 \times \mathbf{e}'_2$, for which we find

$$\mathbf{r}_D = \tau \mathbf{e}_1 + \kappa \mathbf{e}_3 = \mathbf{d}, \quad (4)$$

so that it agrees with the Darboux vector \mathbf{d} of \mathbf{c} 's Frenet frame. For our application, it is problematic if the ruling is too close to the central curve. Hence, one needs to avoid a too small curvature κ .

We are interested in placing D either tangential or normal to a given reference surface S with $\mathbf{c} \subset S$:

- Tangential placement of D implies that \mathbf{c} 's rectifying planes are tangential to S . Hence \mathbf{c} 's osculating planes are normal to S and \mathbf{c} is a geodesic curve on S . We speak of a *geodesic strip* tangent to S . In the Darboux frame of \mathbf{c} w.r.t. S , its rulings have direction vectors $\mathbf{r}_D = \tau_g \mathbf{e}_1 - \kappa_n \mathbf{u}$. Hence, for our practical purposes, the strip should not get too close to an asymptotic direction (where $\kappa_n = 0$).
- If we place the strip orthogonal to S along \mathbf{c} , the tangent planes of D (rectifying planes of \mathbf{c}) are orthogonal to the tangent planes of S . Hence, the osculating planes of \mathbf{c} are tangent to S and \mathbf{c} is an *asymptotic curve* of S . Now we can set $\mathbf{e}_2 = \mathbf{u}$, $\mathbf{e}_3 = \mathbf{n}$ and obtain as ruling vector of D in the Darboux frame notation $\mathbf{r}_D = \tau_g \mathbf{e}_1 + \kappa_g \mathbf{n}$. The ruling agrees with the surface normal only for $\tau_g = 0$, characterizing a principal direction. However, we have an asymptotic curve, which can be principal only if it is a straight line with a constant tangent plane along it, for example a ruling on a developable surface. This is not the case in our application. Since we want a ruling not too close to the tangent, we need sufficiently high $\kappa_g = \kappa$.

2.3. Special surface parameterizations and webs

The main structures of interest are webs of geodesic (G) and asymptotic (A) curves on a surface S (see Fig. 4). A curve $\mathbf{c} \subset S$ which is geodesic *and* asymptotic is a straight line. This case is not of interest here, since one cannot place a developable strip tangential or orthogonal to S along a straight line $\mathbf{c} \subset S$, unless the tangent planes of S are constant along \mathbf{c} . That would be true for rulings \mathbf{c} of a developable surface S . However, we aim at modeling double curved surfaces S .

We start with a parametric representation $\mathbf{s}(u, v)$ of S and extend the net of isoparameter curves $u = \text{const.}$ and $v = \text{const.}$ by diagonal curves $u + v = \text{const.}$ and/or $u - v = \text{const.}$ to a web. Our main interest is on 3-webs of type (AAG) and (AGG):

- The construction of an *AAG-web* will start from a surface parameterization in which both isoparameter lines are asymptotic curves. Such an asymptotic parameterization $\mathbf{s}(u, v)$, or shortly called *A-net*, requires the osculating planes of isoparameter curves being tangential, i.e.

$$\mathbf{s}_{uu} \cdot \mathbf{n} = 0, \quad \mathbf{s}_{vv} \cdot \mathbf{n} = 0, \quad (5)$$

where lower indices u, v indicate partial derivatives with respect to u and v , respectively. There isn't much freedom in an asymptotic parameterization of a given negatively curved surface S . Any two are related by admissible reparameterizations of the form $u = f(\bar{u}), v = g(\bar{v})$. This does not leave sufficient freedom to achieve that diagonal curves are geodesics. Hence, AAG-webs exist on special surfaces only. Simple surfaces which carry an AAG-web are all negatively curved rotational surfaces. Here the web is formed by the two families of asymptotic curves and the profiles in planes through the rotation axis. This follows by symmetry with respect to each profile plane.

- *AGG-webs* possess slightly more degrees of freedom, since the geodesics form a 2-parameter family of curves on a surface, while the asymptotic curves are determined. Despite that, there is still a shape restriction, which can already be guessed from the fact that GGG-webs restrict the shapes, whose classification is missing, as is the case for surfaces which carry an AGG-web. Simple examples of surfaces with AGG-webs are certain developable surfaces obtained as follows: Select one family of lines in a 3-web of straight lines in the plane, using the explicit representation of Graf and Sauer [10]), and map them by isometric deformation to the rulings of a developable surface S . The rulings are the asymptotic curves of S and the isometry maps the other two line families in the planar web to geodesics on S .

A characterization and classification of surfaces which carry AAG or AGG-webs appears to be difficult and is beyond the scope of the present paper.

3. Computation based on discretization and optimization

Having outlined the basic facts from geometry, we are now able to turn to the computational design of hybrid asymptotic geodesic gridshells. We use concepts from discrete differential geometry [16], modeling with freeform curves and numerical optimization. We first provide an overview of the computational pipeline and then elaborate on the individual steps in detail.

3.1. Overview of the computational approach

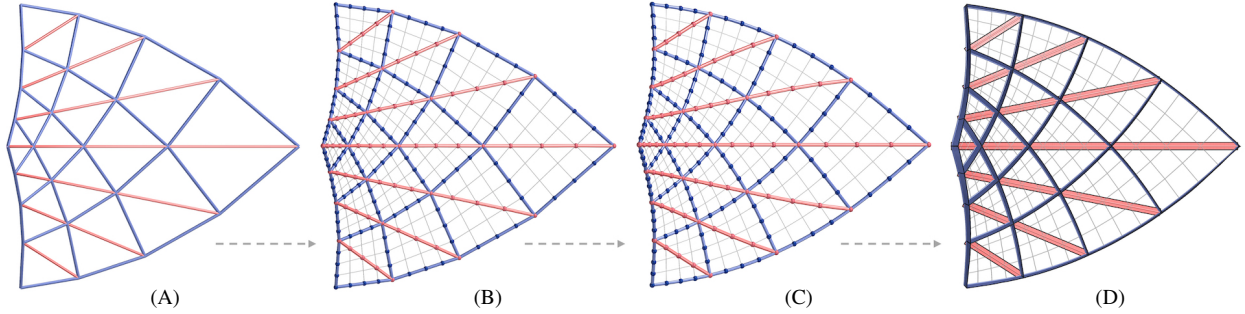


Figure 7: Overview of the computational approach. (A) coarse web (here, an AAG-web; A=blue, G=red). (B) refined web after applying subdivision twice. (C) relevant polylines on the refined mesh are optimized so that they possess the required properties (asymptotic or geodesic). (D) AAG network from three families of developable strips.

The webs we have discussed so far are based on dense families of smooth curves on a smooth surface. We actually need only a discrete family of curves on an underlying smooth surface. Since the knowledge on the specific webs in the smooth setting is very limited, we use a discrete approach. We first compute a coarse discrete version of a targeted web. For a 3-web, this is a triangle mesh with regular combinatorics in which the three families of main polylines have the required meaning (asymptotic or geodesic) in the sense of discrete differential geometry (Fig. 7(A)). This discrete web is then refined via subdivision (Fig. 7(B)) and optimized so that only the original, but now refined polylines have the required properties (Fig. 7(C)). Finally these polylines are approximated by C^3 -spline curves whose segments are Bézier curves of degree 5. Here, we also compute the rulings of associated developable strips. The final result is a web of developable surface strips with straight development, which are tangent to the underlying surface (represented as a quad mesh) along the geodesic curves in the web and orthogonal along the asymptotic curves in the web (Fig. 7(D)).

3.2. Discrete nets and webs of asymptotic and geodesic curves

The discrete version of a curve is a polyline with vertices \mathbf{v}_i . Its edges $\mathbf{v}_i\mathbf{v}_{i+1}$ are discrete tangents and the planes spanned by three consecutive vertices $\mathbf{v}_{i-1}\mathbf{v}_i\mathbf{v}_{i+1}$ are discrete osculating planes [15].

A discrete net is defined by a map $f : \mathbb{Z}^2 \rightarrow \mathbb{R}^3$ and thus a quad mesh with regular combinatorics. The discrete parameter lines through $(u, v) \in \mathbb{Z}^2$ are polylines $f(\mathbb{Z}, v)$ and $f(u, \mathbb{Z})$, which we call u -lines and v -lines like in the smooth case. Our interest is in those discrete nets in which both families of discrete parameter lines are asymptotic or geodesic.

A *discrete asymptotic parameterization* of a surface is a quad mesh in which at each vertex the discrete osculating planes of the discrete u -line and of the discrete v -line agree. Hence, it is a quad mesh with *planar vertex stars*, i.e., a quad mesh where a vertex \mathbf{v} and its four connected neighbors \mathbf{v}_i , $i = 1, \dots, 4$ lie in a plane (Fig. 8(A)). These A -nets are well studied in discrete differential geometry [16] and share many properties with their smooth counterparts. The constraint of planar vertex stars is the discrete version of Eq.(5). We formulate it with help of an auxiliary variable \mathbf{n} , representing the unit normal vector at \mathbf{v} , as

$$\mathbf{n} \cdot (\mathbf{v}_i - \mathbf{v}) = 0, \quad i = 1, \dots, 4. \quad (6)$$

$$\|\mathbf{n}\|^2 = 1. \quad (7)$$

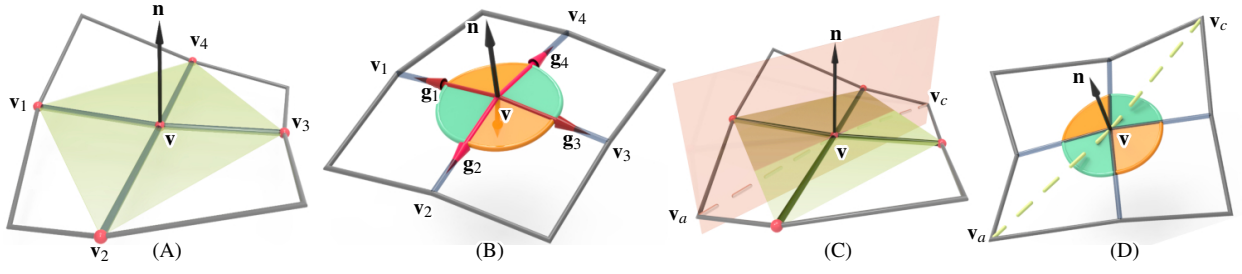


Figure 8: Constraints at vertex stars for various types of nets and webs. (A) An A-net has planar vertex stars; the five vertices $\mathbf{v}, \mathbf{v}_i (i = 1, \dots, 4)$ are coplanar. (B) Equal opposite angles at a vertex of a G-net. The vertex normal \mathbf{n} bisects edge vectors $\mathbf{g}_1, \mathbf{g}_3$ and $\mathbf{g}_2, \mathbf{g}_4$. (C) An AAG-web is obtained from an A-net by adding a family of diagonal polylines so that they are discrete geodesic curves. This requires the vertex normal \mathbf{n} to be coplanar with diagonals $\mathbf{v}_a - \mathbf{v}$ and $\mathbf{v}_c - \mathbf{v}$. (D) An AGG-web is obtained from a G-net by adding a family of diagonal polylines so that they are discrete asymptotic curves. This requires the vertex normal \mathbf{n} to be orthogonal to edges $\mathbf{v}_a - \mathbf{v}$ and $\mathbf{v}_c - \mathbf{v}$.

265 The normalization of \mathbf{n} is important, since otherwise during optimization \mathbf{n} can converge to the zero vector and thus fulfill Eq.(6) without expressing coplanarity.

The construction of AGG-webs is based on *discrete geodesic nets (G-nets)* in which both families of discrete parameter lines are geodesics. Such G-nets appeared at various places in the literature, probably for the first time in a paper by W. Wunderlich [17], and most recently in work by Rabinovich et al. [18, 19] on discrete developable surfaces, modeled via orthogonal G-nets. The constraint for G-nets is also at vertices and requires that opposite angles in each vertex star agree (see Fig. 8(B)). With normalized direction vectors of the edges emanating from vertex \mathbf{v} ,

$$\mathbf{g}_i = (\mathbf{v}_i - \mathbf{v}) / \|\mathbf{v}_i - \mathbf{v}\|, \quad i = 1, \dots, 4, \quad (8)$$

this amounts to the condition

$$\mathbf{g}_1 \cdot \mathbf{g}_2 = \mathbf{g}_3 \cdot \mathbf{g}_4, \quad \mathbf{g}_2 \cdot \mathbf{g}_3 = \mathbf{g}_4 \cdot \mathbf{g}_1. \quad (9)$$

Such a vertex star has the property that the discrete osculating planes of parameter lines intersect in a line which deserves to be called a discrete normal at the vertex: For both discrete isoparameter lines meeting there it is a bisecting line of the two edges through \mathbf{v} . In other words, the rotation by 180 degrees about that normal maps the vertex star in itself. Thus, the computation of a (non-normalized) normal vector $\bar{\mathbf{n}}$ at \mathbf{v} can be based on one of the following equations,

$$\bar{\mathbf{n}} = \mathbf{g}_1 + \mathbf{g}_3 \quad \text{or} \quad \bar{\mathbf{n}} = \mathbf{g}_2 + \mathbf{g}_4. \quad (10)$$

There is an alternative way to compute a vertex normal: The two geodesic polylines through \mathbf{v} have normals \mathbf{m}_1 and \mathbf{m}_2 of their discrete osculating planes, which must be orthogonal to \mathbf{n} ,

$$\mathbf{n} \cdot \mathbf{m}_1 = 0, \quad \mathbf{n} \cdot \mathbf{m}_2 = 0, \quad \mathbf{m}_1 = (\mathbf{v}_1 - \mathbf{v}) \times (\mathbf{v}_3 - \mathbf{v}), \quad \mathbf{m}_2 = (\mathbf{v}_2 - \mathbf{v}) \times (\mathbf{v}_4 - \mathbf{v}). \quad (11)$$

Discrete AGG-webs. We start with a geodesic net, insert one family of diagonal polylines and express that they are asymptotic (Fig. 8(D)). We use the normal \mathbf{n} at vertex \mathbf{v} , and the two neighboring vertices $\mathbf{v}_a, \mathbf{v}_c$ on the chosen diagonal polyline, and express its asymptotic property by a tangential discrete osculating plane, i.e. one with normal \mathbf{n} ,

$$\mathbf{n} \cdot (\mathbf{v}_a - \mathbf{v}) = 0, \quad \mathbf{n} \cdot (\mathbf{v}_c - \mathbf{v}) = 0. \quad (12)$$

Discrete AAG-webs. Here, we add one family of diagonal polylines to an A-net (Fig. 8(C)). With the unit normal \mathbf{n} at vertex \mathbf{v} , and the two neighboring vertices $\mathbf{v}_a, \mathbf{v}_c$ on the chosen diagonal polyline, we express the geodesic property by a discrete osculating plane containing \mathbf{n} . This requires coplanar vectors $\mathbf{n}, \mathbf{v}_a - \mathbf{v}, \mathbf{v}_c - \mathbf{v}$,

$$\mathbf{n} \cdot [(\mathbf{v}_a - \mathbf{v}) \times (\mathbf{v}_c - \mathbf{v})] = 0.$$

In our optimization framework, we prefer quadratic constraints and thus replace this equation by

$$\mathbf{n} \cdot \mathbf{m} = 0, \quad \mathbf{m} = (\mathbf{v}_a - \mathbf{v}) \times (\mathbf{v}_c - \mathbf{v}). \quad (13)$$

270 *Discrete AGAG-webs.* As illustrated in Fig. 8(C-D), one may apply this to both diagonal polylines and obtain a discrete 4-web, which we call an AGAG-web. As we will see later, it is possible to obtain numerically sufficiently accurate results. However, the existence of a precise solution of the constraint system and of the smooth counterparts is not proven. In fact, a count of degrees of freedom raises doubts. If such exact solutions exist, the variety of possible shapes is certainly small.

275 By construction, the two diagonal quad meshes of the A-net in an AGAG-web are geodesic nets with planar faces. Hence, they are discrete versions of conjugate geodesic nets, first studied by A. Voss [14]. These Voss nets have the remarkable property that they possess isometric deformations which keep them geodesic and conjugate. While the preservation of the geodesic property under an isometry is clear, the preservation of the conjugacy relation is very unexpected, as it is expressed via the second fundamental form. Discrete Voss nets are remarkable examples of flexible quad meshes with rigid planar faces. They are also reciprocal parallel nets to discrete surfaces of constant negative Gaussian curvature (see e.g. [15, 17, 50]), which can be covered by planar quad panels; see Montagne et al. [51]. Unfortunately, one cannot show that a Voss net may always be extended to an AGAG-web, which is already expected from the fact that there are also positively curved Voss nets.

3.3. Optimization

285 Having provided the constraints to be imposed on the various types of discrete structures we are interested in, we now turn to the numerical solution of the arising systems of constraints. We apply the *guided projection algorithm* [52], which is an appropriately regularized Gauss-Newton method. It uses auxiliary variables in order to have constraints that are at most quadratic.

Besides all vertices \mathbf{v} of the mesh as variables, normals \mathbf{n} at \mathbf{v} and binormals \mathbf{m} of geodesic polylines are extra variables. The constraints for AGG-, AAG- and AGAG-webs are summarized in Table 1. Almost all constraints

Webs	Variables	Constraints
AGG	\mathbf{v}	(9),(10),(12)
AAG	$\mathbf{v}, \mathbf{n}, \mathbf{m}$	(6),(7),(13)
AGAG	$\mathbf{v}, \mathbf{n}, \mathbf{m}_1, \mathbf{m}_2$	(6),(7),(9),(11)

Table 1: Optimization constraints for hybrid webs.

are quadratic, except for (8). There, we simply take the norms of edge vectors $\|\mathbf{v}_i - \mathbf{v}\|$ from the previous iteration. Moreover, we insert (8) into (9) and therefore the edge vectors \mathbf{g}_i do not appear as auxiliary variables in our optimization.

290 *Fairness.* Our target is to get discrete webs that resemble webs of smooth curves on smooth surfaces. The above hard constraints are in general not sufficient to achieve that, unless the initial mesh for the optimization is already close to a final solution. Therefore, we adopt a fairness energy of mesh polylines. We use the standard approach by adding vanishing squared second differences $\mathbf{v}_{i+1} - 2\mathbf{v}_i + \mathbf{v}_{i-1} = 0$, applied to all polylines forming the web, as soft constraints into the final objective function (14).

Controlling the change of vertices. If the initial mesh is far from fulfilling at least one of the hard constraints of the targeted type of web, we add a self-closeness constraint: Mesh vertices $\mathbf{v}^{(j-1)}$ from the previous iteration should not change much when going to the next iteration,

$$\mathbf{v}^{(j-1)} - \mathbf{v}^{(j)} = 0.$$

295 For interactive manipulation of a web, we gradually change the location of selected vertices \mathbf{v}_s to new positions \mathbf{v}_s^n , via the constraint $\mathbf{v}_s - \mathbf{v}_s^n = 0$ (see Fig. 11 and 16).

Proximity to curves or surfaces. If selected vertices \mathbf{v}_p of the mesh are constrained to a plane, defined by its normal \mathbf{n}_p and a point \mathbf{p} , they satisfy

$$(\mathbf{v}_p - \mathbf{p}) \cdot \mathbf{n}_p = 0.$$

If selected vertices \mathbf{v}_p shall stay close to a reference surface Φ , we compute for the current position of \mathbf{v}_p the closest point $\mathbf{p} \in \Phi$, the unit normal \mathbf{n}_p of Φ at \mathbf{p} and add the above constraint. It expresses proximity to the tangent plane of Φ

at \mathbf{p} , which is known as a good approximation of the squared distance function to Φ for points close to Φ [53]. The closest point computation has to be repeated after each iteration. Analogously, if a vertex \mathbf{v}_p shall glide along a given curve c , we require it to be on the tangent (direction vector \mathbf{t}_c) at the closest point \mathbf{p}_c of the curve, i.e.

$$(\mathbf{v}_p - \mathbf{p}_c) \times \mathbf{t}_c = 0.$$

Target function. Above hard constraints $C_i(X) = 0$ from Table 1 and the various additional terms are put into a non-linear least squares problem with the objective function

$$F(X) = \sum C_i(X)^2 + \omega_1 \sum K_j(X)^2 + \omega_2 \sum V_k(X)^2 + \omega_3 \sum P_l(X)^2 + \varepsilon(X - X_c)^2, \quad (14)$$

where X_c contains the current values of all variables X . $K_j(X)$ collects the fairness terms, $V_k(X)$ belongs to vertex control and $P_l(X)$ to proximity constraints.

Choice of weights. We set $\varepsilon = 0.001$. Fairness is a soft constraint and we set its weight to $\omega_1 = 5e - 4$ during the initial iterations. Their number depends on how far the initial mesh deviates from the targeted constraints. Once the optimization achieves a residual value below a certain threshold (we use $1e - 6$), we run 2-5 more iterations with $\omega_1 = 0$ and then terminate the process. If self-closeness is turned on, the weight is initially $\omega_2 = 0.01$ and we use $\omega_1 = 5e - 3$ during the initial iterations, until the preferred residual value is achieved. Then, we run 2-5 iterations with $\omega_2 = 0$, $\omega_1 = 5e - 4$, and finally 2-5 iterations with $\omega_1 = \omega_2 = 0$ and stop the process. The proximity weight ω_3 is set based on the user's preference. A higher value of ω_3 produces closer proximity to the targeted curves or surfaces, at the cost of a higher deviation from the hard constraints. For the examples involving proximity in this paper, ω_3 starts with 0.1 and then turns to 0 in the final iterations. The changes of weights ω_1 , ω_2 and ω_3 can be set and incorporated into the algorithm before starting the optimization. Details for selected figures are listed in Table 2.

Initialization. Since the present optimization problem is nonlinear and non-convex, a good initialization is important. A safe approach is to use explicitly known AAG- or AGG-webs to special shapes to initialize a modeling session and then deform that shape by interactive editing operations. A basic editing operation is to gradually move vertices to new positions, while keeping a few other vertices nearly fixed (soft constraint with low weight). One can also try to attract a selected boundary to a given curve or to a given plane. From a mathematical perspective, this approach uses optimization to navigate in the constraint manifold M_C starting already from a position in M_C . The details for AAG- and AGG-webs are as follows:

AAG-webs are initialized with negatively curved rotational surfaces R . There, the asymptotic curves and meridians (in planes through the axis) form an AAG-web. If the surface is given in parametric form, one can compute a single asymptotic curve as a polyline by integrating the differential equation of asymptotic curves, and forming a web from rotated and reflected copies of it. This yields an A-net with a discrete rotational symmetry and one family of diagonal polylines in planes through the rotational axis. Prior to further manipulation, one may cut it open or select just a part of the initial AAG-web.

AGG-webs can be initialized with developable surfaces as discussed in Section 2.3. An AGG-web on a developable surface consists of the rulings (asymptotic curves) and two further families of geodesics. In the planar unfolding, such a web consists of straight lines, which can be designed using the explicit results of Graf and Sauer [10]. We implemented the case of a cylinder with the simplest web on it, namely one which consists of three families of parallel lines in the planar unfolding of the cylinder and includes the rulings (see Fig. 9). During shape modification of this cylindrical AGG-web, we keep the asymptotic property of the rulings, but make sure that they become curved, and of course we keep the geodesic property of the other two families of geodesics.

A less safe, but sometimes successful approach for initialization is to start with an A-net or a G-net in which one family of diagonals is then optimized to the required G- or A-property, respectively. We tried this with A-nets representing certain minimal surfaces (Fig. 10) and in some cases optimization has been successful, even when asking for an additional property like planarity of a selected boundary polyline, or keeping a non-trivial topology.

Recall the following well-established procedure: In order to get an A-net on a given negatively curved surface, one can compute asymptotic directions, e.g. by the Rhinoceros3D plugin *Bowerbird* [44, 45] and then re-mesh the surface along this guiding field with a quad-remeshing algorithm. There, we prefer to use the *libigl* [54] implementation of mixed-integer quadrangulation (MIQ)[55]. Subsequent optimization for planar vertex stars will only slightly change that mesh and result in an A-net, which may then be further optimized towards an AAG-web.

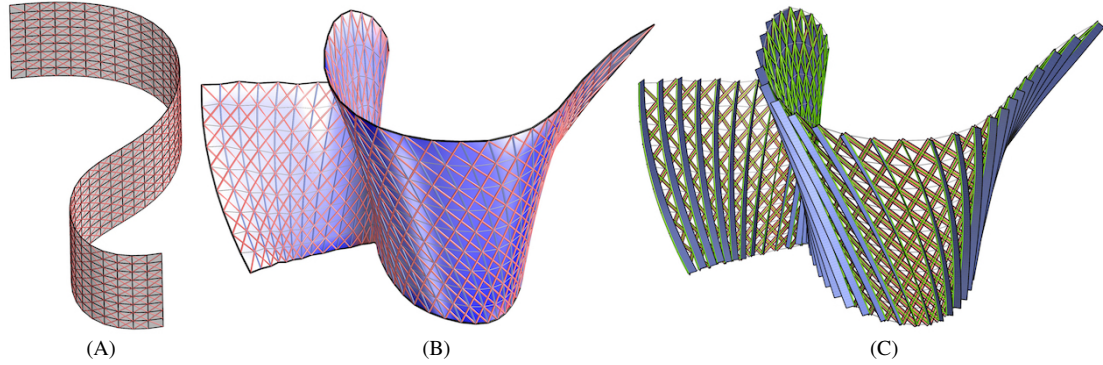


Figure 9: AGG-webs optimized from a developable surface. (A) A cylindrical AGG-web, which is isometric to a planar rectangular mesh with straight diagonals. (B) AGG-web obtained from the initial cylindrical web by interactive editing. The surface is colored by Gaussian curvature: $K < 0$ (blue) and $K = 0$ (white). (C) Designed AGG-web with developable strips.

Fig.	vertices	variables	ω_1	ω_2	ω_3	T/iter	err= $F(X_{\min})$
7(C)	289	1947	$5e-4 \rightarrow 0$	0	0	0.068s	$2.8e-22$
10(B)	308	2436	$5e-3 \rightarrow 5e-4 \rightarrow 0$	$0.01 \rightarrow 0$	$0.1 \rightarrow 0$	0.071s	$4.0e-14$
11(D)	169	1233	$5e-4 \rightarrow 0$	0	0	0.056s	$2.3e-12$
12(A)	725	7764	$5e-4 \rightarrow 0$	0	0	0.029s	$3.2e-12$
13(A)-down	420	4302	$5e-4 \rightarrow 0$	0	0	0.015s	$1.3e-8$
13(B)-up	1037	8421	$5e-4 \rightarrow 0$	0	0	0.018s	$2.8e-19$
13(C)-up	450	4626	$5e-4 \rightarrow 0$	0	0	0.21s	$3.8e-11$
13(C)-down	645	6732	$5e-4 \rightarrow 0$	0	0	0.3s	$1.2e-10$
14	661	4755	$5e-4 \rightarrow 0$	0	0	0.011s	$1.1e-12$
17(A)	160	1248	$5e-3 \rightarrow 5e-4 \rightarrow 0$	$0.01 \rightarrow 0$	$0.1 \rightarrow 0$	0.07s	$1.9e-16$
20(A)	341	2589	$5e-3 \rightarrow 5e-4 \rightarrow 0$	$0.01 \rightarrow 0$	$0.1 \rightarrow 0$	0.081 s	$4e-20$

Table 2: Optimization statistics to selected Figures of different complexity. The initial meshes we use all have a unit-length diameter of their bounding boxes. The algorithms are implemented in Python and tested on an Intel Xeon E5-2687W 3.0 GHz processor.

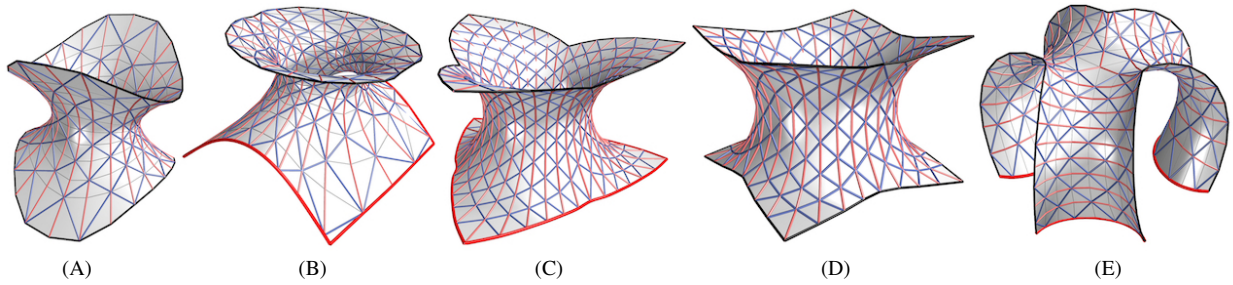


Figure 10: AAG-webs optimized from classical minimal surfaces. Part of their boundary curves (red) are constrained to be planar or linear. (A)-(B) Initial mesh from a *Scherk tower surface*. (B) Two bottom boundary curves are linear and another two planar. (C) Initialized from part of a *Schwarz H surface*. Bottom boundaries are coplanar. (D)-(E) Initial mesh from a *Schwarz P surface*. (E) Coplanar bottom boundary curves.

Example for deformation and verification. We start with a discrete version of a rotational surface of constant Gaussian curvature $K < 0$ (Fig. 11). The A-net in this case has constant edge length. It is known that A-nets with constant edge length can discretize any surface of constant negative Gaussian curvature (see e.g. [16, 17]). The A-net is extended to an AAG-web by polylines in planes through the rotational axis.

We tested the flattening process of an AAG-web, by keeping the AAG property and edge lengths of the A-net, but allowing the G-net to change length. The simulation yielded accurate results: The geodesic planks adjust their length and become straight in the planar state. There, the A-net is formed by cylindrical strips orthogonal to the ground. A

345 similar experiment was conducted and verified physically in Section 4.1.

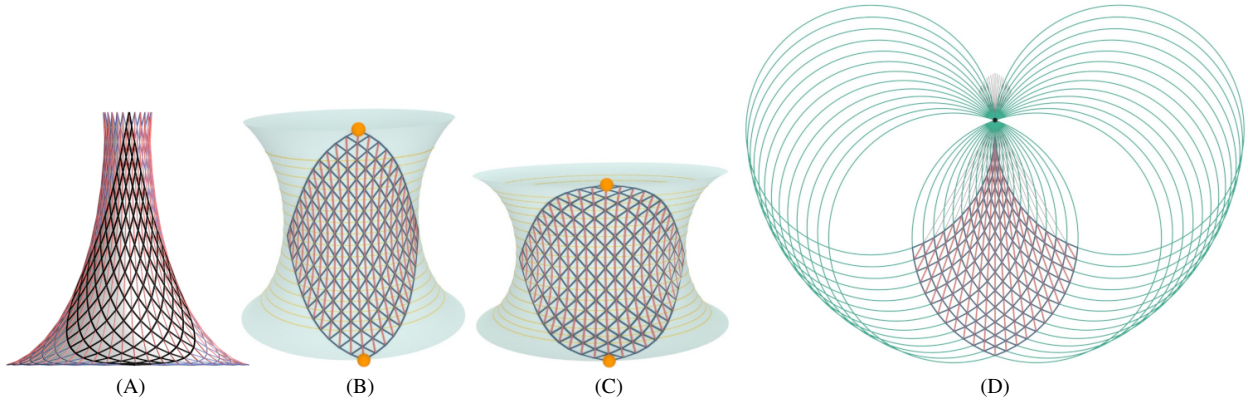


Figure 11: Flattening a rotational AAG-web by keeping the AAG property and edge lengths of the asymptotic net in the web. These edge lengths are constant in the present case, implying that each position of the web represents a surface of constant negative Gaussian curvature K (the value of K is changing during deformation and zero in step D). (A) The black patch of the rotational AAG-web is selected. (B)-(D) States of a deformation achieved by interactive editing. They lie on rotational surfaces. State (D) is planar and thus the geodesics are straight. The asymptotic curves in the planar state lie on congruent circles.

This example is also a good test for the accuracy of our discrete model and optimization for the following reason: *All obtained webs must represent discrete rotational surfaces with constant Gaussian curvature K , but different values of K at different states.* This follows by the symmetries of faces. Each face is a skew rhombus (quad with equal edge lengths) and symmetric with respect to two orthogonal planes. Each of these symmetry planes is spanned by one diagonal and contains the normals at its end points. These normals are present in the A-net and must agree for faces sharing a vertex. For those diagonals, which form geodesic polylines, also the symmetry planes must agree. Hence, an entire strip of quads sharing a geodesic polyline P_G is symmetric with respect to plane of P_G . This holds for all geodesic polylines and immediately shows the discrete rotational symmetry. *Moreover, the limit positions of the asymptotic polylines in the planar state lie in general on congruent circles. These contain the common point of the lines on which the geodesics of the planar web lie.* The proof is again simple: As a limit of rotational symmetric webs, the planar state also has rotational symmetry. There, the straight geodesic polylines (red lines in Fig. 11) must pass through a common point C . Moreover, we have a net of congruent rhombuses in the plane. Thus, it is formed by translating a polyline with constant edge length against another one. These are the limit positions of the asymptotic polylines (blue in Fig. 11). Because of the rotational symmetry, each edge of such a polyline appears from the center C under constant angle and therefore all its vertices lie on a circle through C .

A further special planar limit state of Figure 11 has parallel asymptotic and geodesic strips, thus forming a regular grid. A similar physical experiment was conducted and digitally modelled in Section 4.1.

Another example, even more closely related to that experiment, is the editing example of Fig. 16.

3.4. Subdivision and extraction of strips

Refinement through subdivision. So far, we only described the most important step A in the entire computational approach (see Fig. 7). This is followed by a simple subdivision through bilinear interpolation of the individual quads (Fig. 7(B)). We then optimize the refined mesh so that the originally already present discrete curves (now refined) keep their properties of being discrete asymptotic or geodesic curves (blue and red polylines in Fig. 7(C)) on the refined surface (grey mesh in Fig. 7(C)). There, we can use the constraints for asymptotic or geodesic polylines discussed in Section 3.2. However, we have to define the vertex normals \mathbf{n} in another way. Here, we simply require \mathbf{n} to be discrete normals to the other mesh polylines through \mathbf{v} . If \mathbf{v}^- and \mathbf{v}^+ are the two neighboring vertices of \mathbf{v} on such a polyline, we add the constraint

$$(\mathbf{v}^- - \mathbf{v}^+) \cdot \mathbf{n} = 0.$$

365 As a result of step C in our overall process, we have the basic polylines for the strips which form the final gridshell. These are sufficiently well designed discrete curves, from which one may directly extract the strips with help of the

rectifying developable surfaces (Section 2.2). While this process can also be done in a discrete fashion, we describe in the following an alternative based on splines. This is also useful for integration into a NURBS-based modeler.

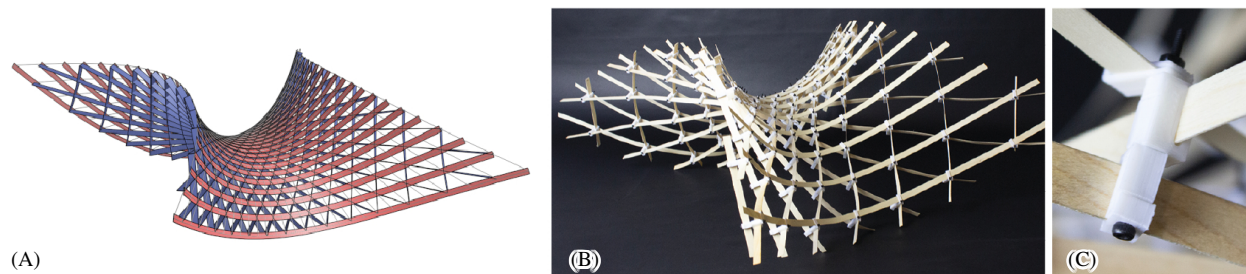


Figure 12: The computed mesh (A) was used to create a physical verification model (B). For this purpose, straight slats were connected laterally with hinged 3D joints.

370 *Extraction of strips.* Each discrete asymptotic or geodesic polyline arising from step C is now interpolated by a C^3 -spline curve $\mathbf{c}(t)$ composed of Bézier curves of degree 5. Their end points are exactly the nodes of the web, where we make sure that the osculating plane is tangent (A) or orthogonal (G) to the reference mesh. Together with the linear C^3 constraints at nodes, a standard least squares approximation (see [56]) is applied.

Due to C^3 smoothness we obtain a continuous sequence of rulings in the developable strips, since the direction vectors of rulings are given by the Darboux vectors $\mathbf{r}_D = \tau \mathbf{e}_1 + \kappa \mathbf{e}_3$, where torsion τ depends on the third derivative of \mathbf{c} . The computation of these differential geometric quantities for polynomial curves is straightforward. If the strip has width w , we see from its unfolded straight version, that a ruling $r(t)$ meets the given boundary and the other boundary at points $\mathbf{c}(t), \bar{\mathbf{c}}(t)$ of distance $d_r = w / \cos \alpha$, where α denotes the angle of \mathbf{r}_D and the binormal $\mathbf{e}_3(t)$. This yields the following parametric representation of the other boundary $\bar{\mathbf{c}}$,

$$\bar{\mathbf{c}}(t) = \mathbf{c}(t) + \frac{w}{\mathbf{r}_D(t) \cdot \mathbf{e}_3(t)} \mathbf{r}_D(t).$$

375 For a general polynomial curve $\mathbf{c}(t)$, neither the binormal vector \mathbf{e}_3 nor the Darboux vector \mathbf{r}_D are rational in t , and therefore the other boundary $\bar{\mathbf{c}}(t)$ does in general not possess an exact NURBS representation. This is of no concern for the present application. Of course, one can come up with a NURBS approximation of sufficiently high accuracy.

380 The positions of rulings have an influence on the physical realization. If they are not too far away from the surface normals of S , bending will occur roughly along short line segments transversal to the slat. A ruling close to the tangent of \mathbf{c} would indicate diagonal warping of the slat, and result in a curved cross-section at the intersection points. One may see this also from a mechanical perspective. The actual physical realization forces the asymptotic strips through the straight node axis (orthogonal to S) at each joint. This causes the asymptotic strips to twist, and slightly diverge from a purely developable shape.

385 Fig. 12 shows a simple digital model designed with our algorithm and verified by a physical model. Further results obtained with our computational framework are shown in Fig. 13. The shapes are relatively simple, which is partially due to the type of initialization we are currently using. The existence of AGAG-webs of sufficiently high accuracy (see Table 2) comes as a surprise. They have been computed using simple AGG-webs (such as the one in Fig. 13, top left) as initialization, followed by optimization towards the AGAG property.

390 *Mesheres with combinatorial singularities.* So far, our discussion has been confined to nets and webs of regular combinatorics. This limits the shape variety. Note that the A-net of a negatively curved surface has singularities at the flat points of the surface. One can realize some surfaces with flat points by AAG-webs as well. However, certain modifications are required (see Fig. 14). First of all, we note that in a singular vertex of an A-net an even number $N \geq 6$ edges meet ($N = 8$ in Fig. 14). We optimize the web with the presented constraints only at regular vertices. The diagonal geodesics cannot run smoothly over the entire surface, but have to break at N polylines through a singularity. Such break points (tangent discontinuities of an underlying smooth curve) can be modeled by not applying the fairness term there. Essentially, one divides the web into N combinatorially regular AAG-webs.

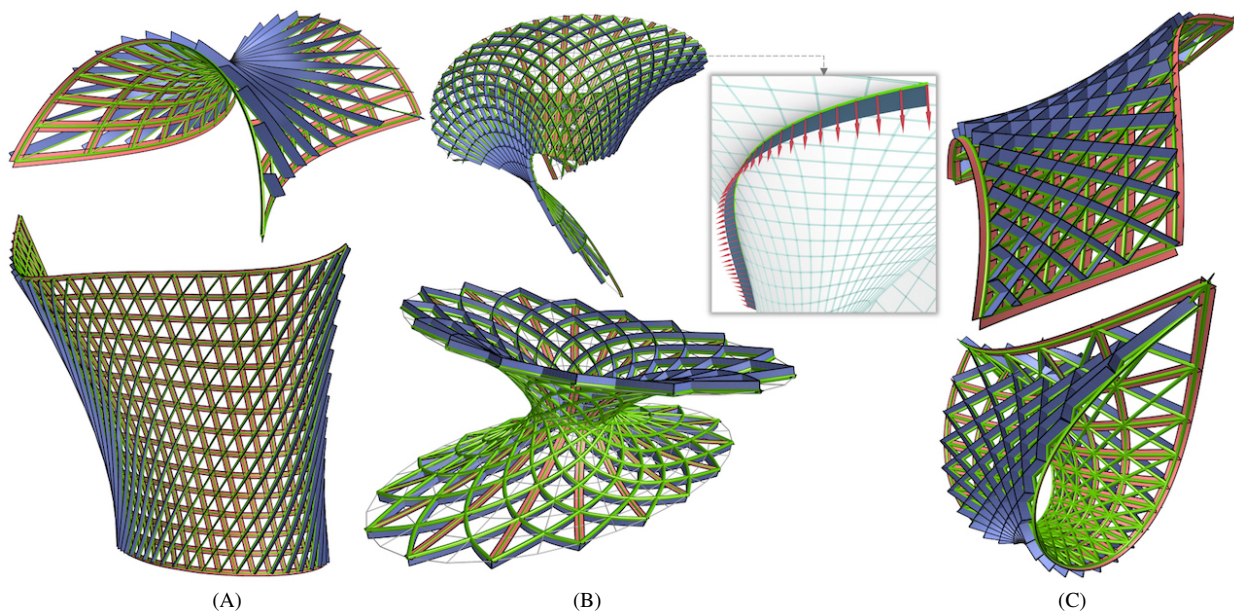


Figure 13: Digital models of various types of asymptotic geodesic hybrid gridshells. Column (A) AGG-webs, column (B) AAG-webs, column (C) AGAG-webs with low numerical errors (see Table 2). A zoom onto one strip, orthogonal to the reference surface, together with the ruling vectors is also shown.

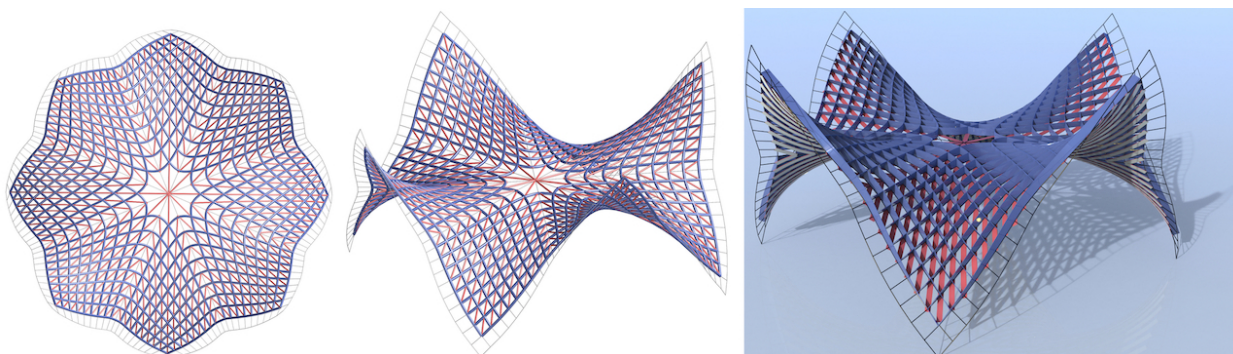


Figure 14: An AAG gridshell with a central combinatorial singularity. Diagonal geodesics break at eight polylines through the singularity.

395 3.5. *Link to the Grasshopper and Rhinoceros3D environment*

A user-friendly design tool has been realized by integrating the optimization into the CAD system Rhinoceros 3D. Our plugin allows the user to define the main inputs to the optimization, the initial mesh, the web type, strip width and optimization parameters like the number of iterations and weights. The results, namely the optimized mesh, strip boundaries in piecewise quintic Bézier form, ruling vectors, the developable strips as well as their developments
 400 are returned as Rhinoceros 3D geometry objects. The optimization is implemented in CPython and called from Grasshopper, Rhinoceros' parametric design extension, using the *Hops* component [57]. This allows the user to offload the actual computation to a more powerful remote machine, if desired. We will make our plugin available to the architectural community in the near future.

4. Architectural investigation

405 Asymptotic-geodesic hybrids offer several benefits for architectural design and construction: The use of standardized
straight slats allow simple fabrication, logistics and transport. The combination of geodesic and asymptotic planks
creates structural stability, through triangulation and the interaction of tall and wide profiles. The geodesic grid offers
effective cladding with standardized, straight press-strips and developable panels. Apart from these functional benefits,
410 the complementary weaving of flat and tall elements has a strong graphical depth and naturally creates an aesthetic
pattern.

In this section, we first conduct a physical experiment to investigate the natural elastic behaviour and form-
generation of AG-nets and gain insights on the erection process of triangulated webs. Then, the computational method
is implemented to design two architectural scenarios in timber and steel that showcase the possible applications of
AG-nets for elastic gridshells and curtain wall design.

415 4.1. Physical experiments

A physical experiment is conducted to form-find AAG-, AGG- and AGAG-webs. For this purpose, a simple joint
was designed, which allows the combination of two vertical and two horizontal lamellas. The joint is printed as a
90-degree intersection with sufficient tolerance to allow up to 5 degrees of play. 5x1 mm timber lamellas are loosely
slotted through the joints to allow sliding and adjusting their length. Three combinations are investigated (see Fig. 15):

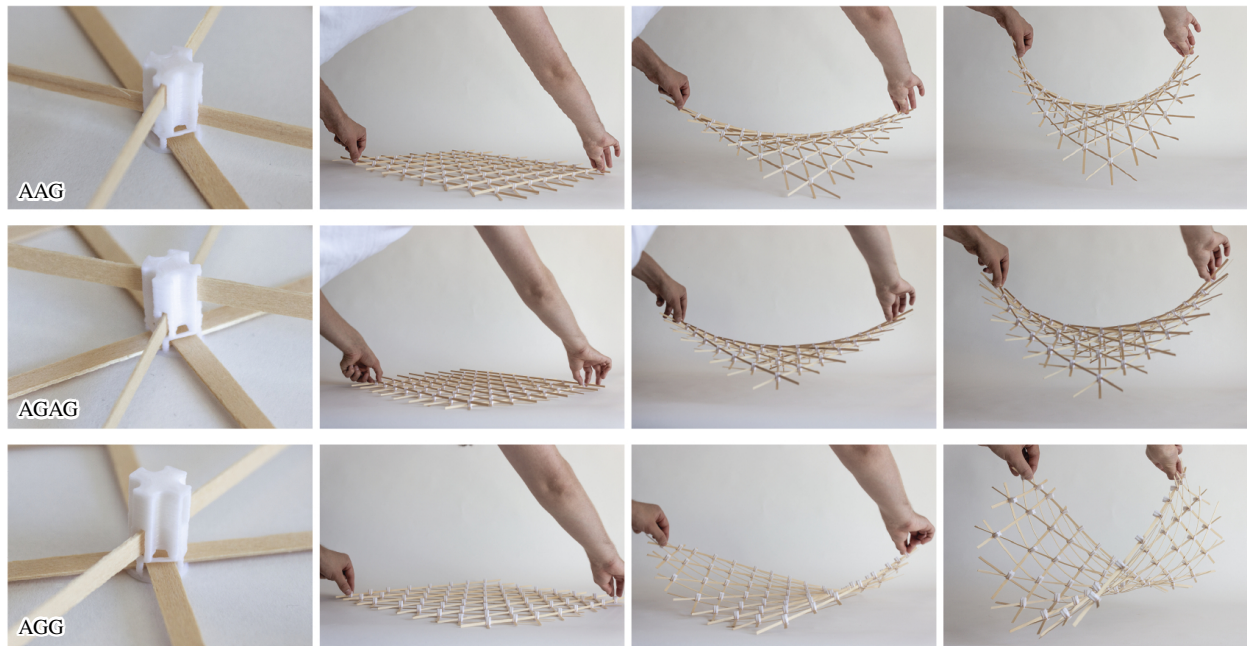


Figure 15: Physical deformation experiment for equilateral AG-webs. AAG- and AGAG-webs naturally deform into a negatively curved shape. AGG-webs naturally seek a nearly developable shape. A similar deformation of an AAG-web was simulated digitally (see Fig. 16)

- 420
- AAG: A regular net of 8 x 8 asymptotic lamellas combined with 13 diagonal geodesic lamellas.
 - AGAG: The same regular grid as AAG, with a second diagonal layer of geodesics.
 - AGG: A regular net of 8 x 8 geodesic lamellas combined with 13 diagonal asymptotic lamellas.

Each of the samples is laid flat on a table and simply lifted up on two opposing corners, to initiate a natural transformation into double curvature.

425 The AAG-web naturally takes on a negatively curved shape with asymptotic curves curving outwards on all four sides. During this experiment, the asymptotic curves shift very little, while the geodesic lamellas noticeable glide through the printed joints, using shorter lengths in the centre and elongating in the corners. The final shape has a high similarity with a rotational surface, as geodesics showed close to no torsion and each remained in a plane. This deformation of an AAG web is also modeled digitally using the editing example Fig. 16. The optimization starts from a planar grid and includes a limited angle change of the 90-degree nodes (imposed by the 3D-printed joints in Fig. 15).
 430 The gliding of slats through the nodes is incorporated into the optimization by allowing a change of edge length, but keeping the total lengths of slats unchanged. From a purely geometric perspective, the obtained shape must be close to part of a rotational minimal surface (catenoid), since the nodes constrain the asymptotic curves to be nearly orthogonal and the geodesics to nearly bisect the asymptotic curves. Hence geodesics must be nearly principal curvature lines. A
 435 geodesic principal curvature lies in a plane which intersects the surface under right angle. This finally yields the near rotational symmetry, seen very well in our experiments.

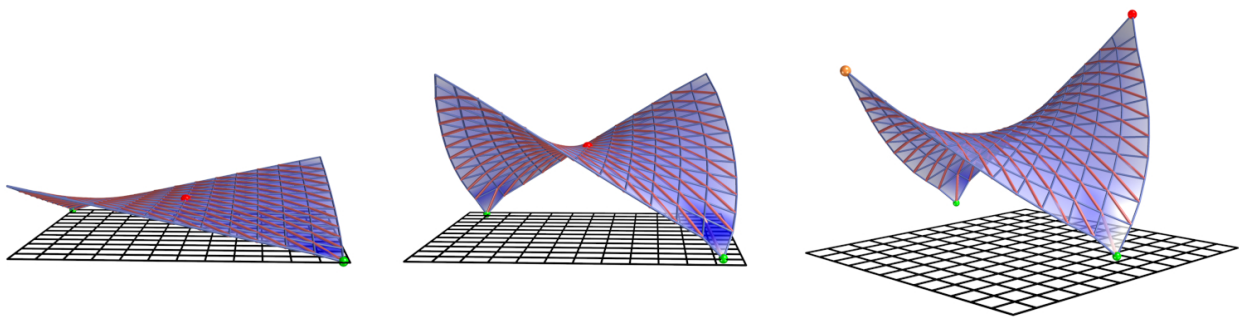


Figure 16: AAG-webs, designed through interactive editing via handle-points. Starting from a planar square grid (initial A-net) with two opposite corner points (green) constrained to the plane (weight 1), we move a central point (red) gradually to produce a sequence of AAG-webs. In addition, we require orthogonal nodes of the A-net (weight 0.1) and keep the total length of each asymptotic polyline and geodesic polyline (weights 1). The green points glide in the starting plane, the orange point is fixed, and the red point is the moving handle. This process simulates the bending experiment of the physical AAG gridshell in Fig. 15.

The AGAG-web shows a much more restricted movement, but does deform into negative curvature, similar to the AAG-sample. Due to the specific nodes, the geometric restrictions of AGAG webs as discussed in section 3.2 are now even more severe: Following up on the discussion of AAG-webs with the present nodes, one needed to have a minimal surface which is rotational with two different axes, and this is not possible. This shows that a purely geometric deformation model is not sufficient. One also needs to consider tolerances at joints and the deformation behavior of the used material.
 440

The AGG-web directly approached a developable shape, where geodesics showed high deformation while the family of asymptotic curves remained nearly straight with a slight s-curve. We attribute this behaviour to the combination of two orthogonal families of geodesics, which are naturally restricted to a developable surface. However, the tolerances in the nodes allowed for skewing of the grid and slight bulging of the shape.
 445

Erection Strategy. The AAG-experiment reveals a simple physical strategy to construct AAG-gridshells: The grid of lamellas can be assembled flat and pushed up in the designed shape, if geodesic lamellas are able to slide through each joint and adjust their node to node length. The architect can make full use of the compliant mechanism of asymptotic slats, and lock the design shape by securing the geodesic joints. This strategy, however, will affect the possible design shapes. We believe that only rotational AAG-webs allow for sliding geodesics from flat to curved. In any other AAG-web, the geodesics either need more tolerance in the joints, or the erection process has to be completed with only the two asymptotic families, and the geodesic family of lamellas is attached later to secure the curved gridshell. The kinetic behaviour of AAG-webs will be investigated in a separate publication comparing physical experiments with digital simulations.
 455

4.2. AAG timber module

The first architectural scenario is investigating a structural timber grid (see Fig. 18). The goal is to design a doubly curved column-and-roof structure using only identical slats and fully utilize the structural benefits of the hybrid web. The design proposal is a quarter portion of a rotational surface, that is cropped by a 4x4 m square boundary. This segment is 2.6 m tall and could be used as a single cantilevering structure, or as a modular unit that can be combined to form a circular structure. The surface is carefully designed as a funnel shape with almost cylindrical geometry at the base. This forces the asymptotic slats to become vertical and efficiently carry loads to the supports. For the same reason, the geodesic slats are arranged vertically and densify towards the supports.

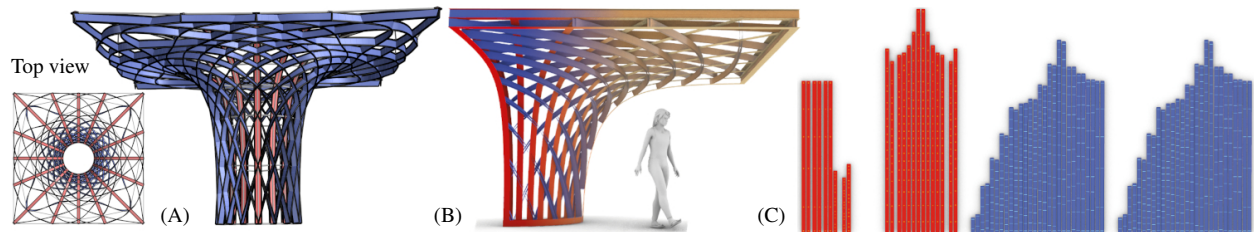


Figure 17: The timber roof structure was designed to be constructed exclusively from straight lamellas, including the edge and support beams. (A) Computed rotational AAG gridshell. Top and bottom mesh boundaries have square and circular shapes, respectively. (B) One quarter of the timber structure. (C) Developments with straight strips.

The innovation of this design lies in the detail. Laminated bamboo slats, with approx. 80x8 mm rectangular cross-section, offer the necessary elasticity and strength for this prototype. Similar to the first timber prototype (see Fig. 2) the two families of asymptotic lamellas are assembled on separate levels so that profiles are continuous. Each asymptotic lamella consists of two slats which are coupled at every joint with rectangular blocks that are cut from the same 80x8 mm timber profile. The double lamella has several advantages: It allows embedding the geodesic curvature during prefabrication, by incorporating the slight differences in node to node distance between inner and outer slat, before laminating them together. The coupling of two lamellas increases the lateral bending stiffness against buckling due to compression or torsion, following a similar strategy as the ribbed shells described in Section 1. Finally, the parallel layout allows to create concentric joints, by inserting two adjacent spacer blocks to define the position of joints as 8x8 mm gaps between the two slats (see Fig. 18(C)).

The two families of lamellas are connected by threading M8, 200 mm bolts through these gaps. This connection acts as a scissor joint and allows rotation of the two families during the erection process. An 8 mm spacer (again using the same material) is added between the top and bottom lamella to avoid friction between asymptotic slats. The spacer also creates the necessary gaps for the diagonal geodesic slats.

Unlike our optimized webs suggest, the geodesics are not assembled from node to node but shifted by half a grid, connecting to the asymptotic slats at mid points between two nodes. This, again, has several advantages: By avoiding the intersection of asymptotic lamellas, the geodesics can be assembled independently. They are interwoven between the top and bottom asymptotic lamellas, either in the flat position or later in the curved shape. This also allows them to slide between the asymptotic lamellas, and thus accommodate for the change in length and additional sideways movement during erection as described in our physical experiments in section 4.1. The connection of geodesics to asymptotics can be tightened independently. The joint functions analogously to the main joints, but with a bolt of half the length, connecting the horizontal slat alternatively to bottom or top lamellas. Once the grid is formed into the correct design shape, the geodesics are fixed and thus triangulate the grid creating a rigid gridshell. Connecting the mid-points of asymptotic lamellas halves their buckling length with significant improvement for the structural behaviour.

The design was verified through a 1:1 joint and a 1:5 model (see Fig. 18). This experimental assembly proved more challenging than expected, as the lamination process of asymptotic double-lamellas increased their bending stiffness and caused higher resistance against bending and torsion during the erection process. Because of this, the geodesics could not be threaded completely in a flat state, but had to be pushed through the structure subsequently during the erection. This model was further reinforced by creating strong edges, with two additional geodesic lamellas added at the



Figure 18: A timber prototype was constructed at 1:5 scale (80 x80 cm). The combination of double asymptotics and interwoven geodesics create a strong web, halves the buckling length and braces the structure. A 1:1 joint was built to test the laminated joints, and bolt connections.

top and bottom. As expected, the final structural grid showed high rigidity. A thorough investigation of the structural behaviour, looking at stability, stiffness, as well as elasticity and strength of timber, will be published in a separate paper.

The two complementary orientations of slats appear like a woven fabric, in which the geodesics act as an interlayer emphasizing the depths of the outer asymptotic lamellas (see Fig. 18(B)). The regularity of joints across this doubly-curved web adds to the strong graphical effect of complexity and order.

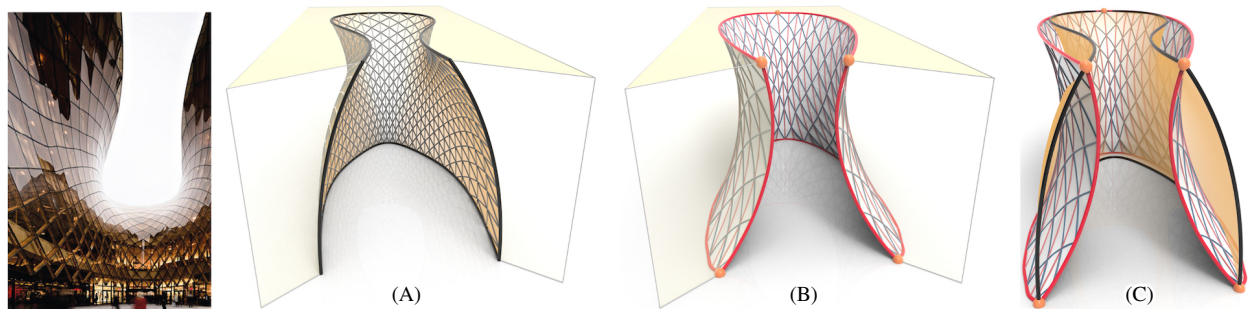


Figure 19: Optimization workflow for the Emporia Shopping Center facade: (A) Original mesh with four planar boundaries. (B) Optimized AAG-web with fixed points and boundaries gliding on the same original planes. The strips are shown in Fig. 20(A). (C) Comparison of meshes (A) and (B).

500 4.3. Steel and glass facade

The second architectural scenario is investigating a multi-story steel and glass facade. The design proposal is inspired by the Emporia Shopping Center Entrance in Malmö (designed by Wingardh Arkitektkontor, 2012). This horseshoe shaped atrium is composed of 473 double and single curved glass panels arranged in a diamond grid. The diagonal grid was remodelled and translated into a symmetric mesh, in order to be rationalized for an AAG-web using the method presented in Section 3(see Fig. 19). The original design surface shows regions of positive Gaussian curvature, which naturally disappeared during optimization and account for the large deviation from the original reference surface. The symmetric surface was finally cropped on one side to fit the original facade (see Fig. 20). A 1:20 model of the design was built from spring-steel strips to verify the feasibility and material behaviour (see Fig. 22).

This new application focuses on the benefits of a deep asymptotic substructure spanning between concrete slabs to resist wind loads. The geodesic layout has several benefits. The mullions brace the façade structure by triangulating the grid. They act as a substructure for the single-curved cold-bent glass panels. A second flat press strip is installed on the outside to clamp the glass panels down and secures the individual curvature. The glass panels themselves follow the geodesic direction and can be produced from flat trapezoidal sheets.

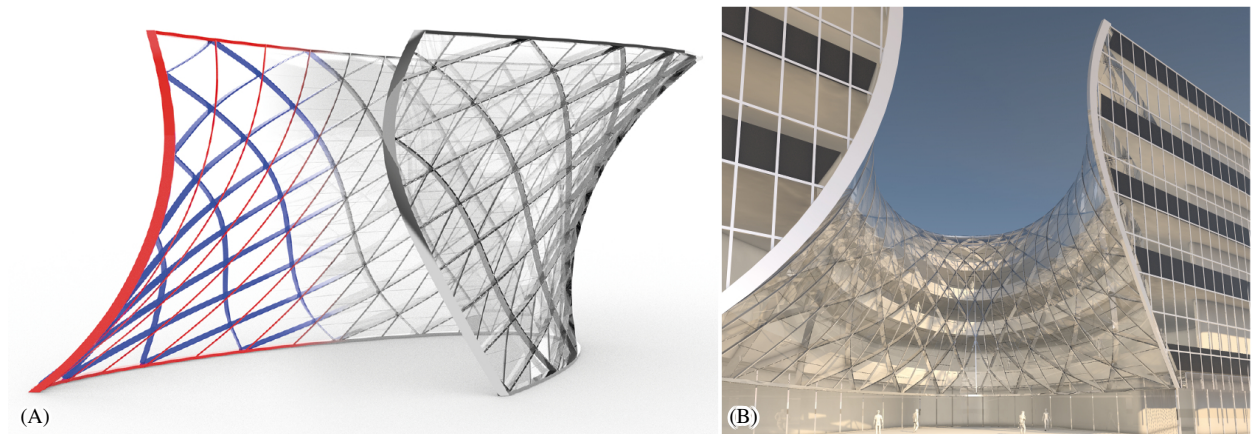


Figure 20: Architectural scenario of a doubly curved steel facade structure with developable glass panels. The design is inspired by the Emporia shopping Center Entrance in Malmö. (A) The strip geometry is used to generate a detailed architectural model of asymptotic double-lamellas, hinged joints and developable facade panels. (B) The facade is integrated as semi courtyard in a rectangular building block.

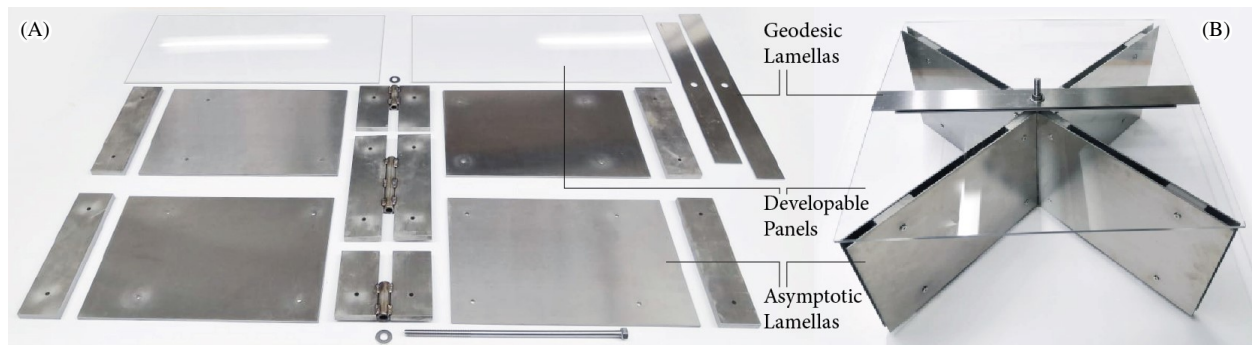


Figure 21: Prototypical steel joint for the doubly curved facade structures (B). All elements can be unrolled flat and straight (A). The asymptotic lamellas are segmented and connected at each intersection through a hinged scissor joint that adjust to the individual intersection angle. The geodesic lamellas acts as the outer mullion system that clamps the developable glass panels.

Each asymptotic beam consists of two steel strips of approximately 5x200 mm (see Fig. 21). The strips are coupled
 515 in regular intervals with steel spacers of approximately 40 mm. These steel composite beams are prefabricated offsite
 from flat sheet material and installed with their final geodesic curvature and torsion embedded. Both asymptotic
 families intersect in one level to reduce the depth of the construction. They are segmented at the intersection points.
 The joint is composed of three steel elements that create a cross-shaped scissor joint and can be used universally for
 all intersections in the asymptotic net. The joint is fixed with a central bolt, which extends outward to connect to the
 520 geodesic mullions. The mullions are extruded aluminium profiles that clamp the developable glass panels.

5. Conclusion

Combining geodesic and asymptotic paths in a doubly curved web, offers rich insights for architectural geometry, design and construction.

525 *Geometry.* The practical considerations naturally led to the new topic of webs on surfaces which consist of geodesic and asymptotic curves. We could provide examples for exact webs and showed how to computationally access the problem using a discrete model based on concepts of discrete differential geometry, and effective techniques for numerical optimization. We could answer some initial questions that come up in connection with the deployment from a planar state.

530 *Design.* The computational method to design AG-nets can be initiated from any asymptotic or geodesic mesh and manipulated interactively by point editing or through boundary conditions to adjust to the designated design shape. The method was tested on open and closed shapes with and without singularities and finally implemented in the design of a timber gridshell module and a doubly curved steel glass façade.

535 *Construction.* The combination of tangential and normal planks in a triangular gridshell creates hybrid benefits for the bracing of the grid structure and its resistance to bending and offers the possibility to use the geodesic mullions as a substructure for developable panels. The deformation of AAG-webs was investigated physically and digitally, and has shown that an elastic erection process from flat to curved is possible for rotational surfaces, if geodesic planks are able to glide through joints and adjust their length. For efficient gridshell construction, the geodesic family of planks can be shifted by half a grid, to avoid the asymptotic intersections, allow independent installation and connect the slender asymptotic lamellas at mid-points to improve their buckling behaviour.

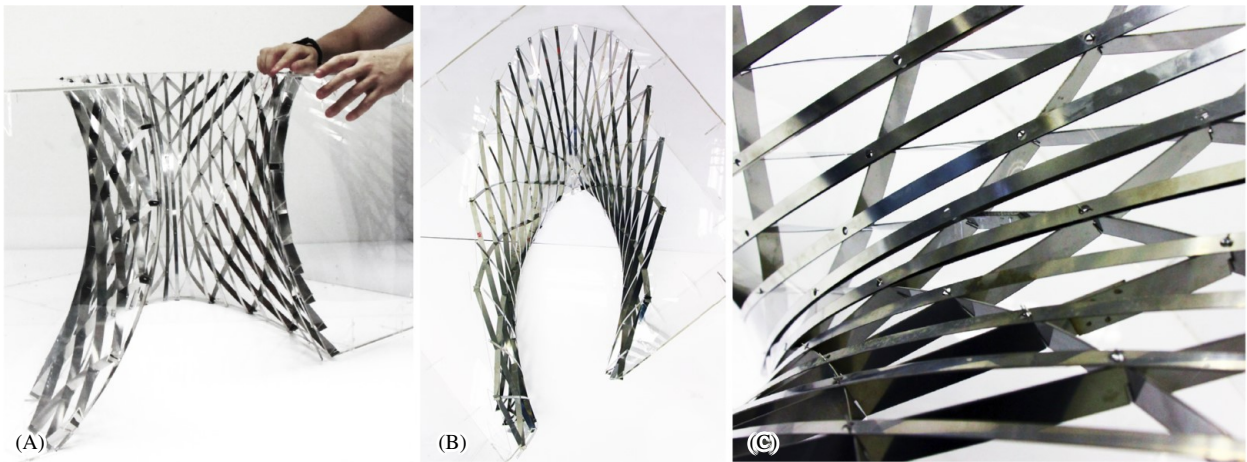


Figure 22: Steel model of the optimized AAG facade structures at scale 1:20, shown in elevation (A), plan (B) and close-up view (C). The two asymptotic families are constructed with slots in the same level. The geodesic lamellas function as triangulation and substructure for the transparent facade panels.

540 *Future research.* In a forthcoming publication, we will report on the generation of discrete AAG- and AGG-webs by an evolution process which starts with an appropriate initial strip and successively adds further strips by keeping the required properties. This type of discrete model generation has been described by R. Sauer [11] for the case of GGG-webs. In this way, one can enrich the variety of starting shapes for further shape manipulation through editing. It will, however, still be difficult to come close to a certain target shape. Therefore, we will also investigate the generation of webs using a level set approach. It plays an important role in the theory of webs [9] and yielded good results for GGG-webs [20]. However, also the level set approach requires an initialization that influences the result. Its choice is not simple. Moreover, we cannot fix the target shape, since the degrees of freedom in creating an AAG or AGG-web (even GGG-web) are not sufficient. Hence, we need to combine the design of the web with a minimal shape change of the reference surface.

550 The kinetic behaviour of AAG-webs for the erection process will be investigated further, by comparing geometric and mechanical simulations with physical experiments. The design and construction of an AAG timber gridshell will help to learn more about the building process, construction details, bending behaviour of wooden planks and structural performance of the asymptotic geodesic grid. We plan to publish these findings in a separate paper.

Acknowledgements

555 This research has been supported by KAUST baseline funding (grant BAS/1/1679-01-01), the Hong Kong Research Grants Council via Early Career Scheme (RGC Ref No. 27604721), and the HKU, University Grants Committee via the Seed-Fund “Repetitive Structures”. We thank Zongshuai Wan, Jacky Chu, Li Xuechang, Liu Yujie and Dominic

Lumley-Smith for their joint effort in producing physical prototypes, visualizations and models. We also like to acknowledge our colleagues from the Technical University in Munich, Chair of Structural Design, Pierluigi D'Acunto and Jonas Schikore for their structural support and interest in this research topic.

References

- [1] H. Pottmann, M. Eigensatz, A. Vaxman, J. Wallner, *Architectural geometry*, *Computers and Graphics* 47 (2015) 145–164.
- [2] S. Adriaenssens, P. Block, D. Veenendaal, C. Williams, *Shell structures for architecture: form finding and optimization*, Routledge, 2014.
- [3] H. Schober, *Geometrie-prinzipien für wirtschaftliche und effiziente schalentragwerke (teil 1)*, *Bautechnik* 79 (1) (2002) 16–24.
- [4] E. Schling, *Repetitive structures*, Ph.D. thesis, Chair of Structural Design, Technical University of Munich, DOI: 10.14459/2018md1449869 (2018).
URL DOI: 10.14459/2018md1449869
- [5] H. Pottmann, *Architectural geometry and fabrication-aware design*, *Nexus Network Journal* 15 (2) (2013) 195–208.
- [6] J. Hennicke, *IL10 Gitterschalen*. Sonderforschungsbereich weitgespannte Flächentragwerke., stuttgart, Institut für leichte Flächentragwerke (1974).
- [7] E. Schling, R. Barthel, Šuchov's bent networks: The impact of network curvature on šuchov's gridshell designs, in: *Structures*, Vol. 29, Elsevier, 2021, pp. 1496–1506.
- [8] S. Finsterwalder, *Mechanische Beziehungen bei der Flächendeformation*, *Jahresber. d. Deutschen Math.-Vereinigung* 6 (1899) 43–90.
- [9] W. Blaschke, G. Bol, *Geometrie der Gewebe*, Springer, 1938.
- [10] H. Graf, R. Sauer, *Über dreifache Geradensysteme*, *Sitz. Bayer. Akad. Math.-nat. Abt.* (1924) 119–156.
- [11] R. Sauer, *Flächen mit drei ausgezeichneten Systemen geodätischer Linien, die sich zu einem Dreiecksnetz verknüpfen lassen*, *Sitz. Bayer. Akad. Math.-nat. Abt.* (1926) 353–397.
- [12] K. Mayrhofer, *Sechseckgewebe aus Geodätischen*, *Monatshefte f. Mathematik u. Physik* 38 (1931) 401–404.
- [13] O. Volk, *Über Flächen aus geodätischen Dreiecksnetzen*, *Sitzungsber. Heidelb. Akad. Wiss. Math.-Natur. Kl.* 1929 (1) (1929) 3–32.
- [14] A. Voss, *Über diejenigen Flächen, auf denen zwei Scharen geodätischer Linien ein conjugirtes System bilden*, *Sitzungsber. Bayer. Akad. Wiss., math.-naturw. Klasse* (1888) 95–102.
- [15] R. Sauer, *Differenzengeometrie*, Springer, 1970.
- [16] A. I. Bobenko, Y. B. Suris, *Discrete differential geometry. Integrable structure*, Vol. 98 of *Graduate Studies in Mathematics*, American Mathematical Society, Providence, RI, 2008.
- [17] W. Wunderlich, *Zur Differenzengeometrie der Flächen konstanter negativer Krümmung*, *Österreich. Akad. Wiss. Math.-Nat. Kl. S.-B. Ila.* 160 (1951) 39–77.
- [18] M. Rabinovich, T. Hoffmann, O. Sorkine-Hornung, *The shape space of discrete orthogonal geodesic nets*, *ACM Trans. Graph.* 37 (6) (2018) 228:1–228:17.
- [19] M. Rabinovich, T. Hoffmann, O. Sorkine-Hornung, *Discrete geodesic nets for modeling developable surfaces*, *ACM Trans. Graph.* 37 (2) (2018) 16:1–16:17.
- [20] H. Pottmann, Q. Huang, B. Deng, A. Schiftner, M. Kilian, L. Guibas, J. Wallner, *Geodesic patterns*, *ACM Trans. Graphics* 29 (4) (2010) 43,1–10.
- [21] B. Deng, H. Pottmann, J. Wallner, *Functional webs for freeform architecture*, *Computer Graphics Forum* 30 (2011) 1369–1378, *proc. Symp. Geometry Processing*.
- [22] J. Vekhter, J. Zhuo, L. F. G. Fandino, Q. Huang, E. Vouga, *Weaving geodesic foliations*, *ACM Transactions on Graphics (TOG)* 38 (4) (2019) 1–22.
- [23] P. Ayres, A. G. Martin, M. Zwierzycki, *Beyond the basket case: A principled approach to the modelling of kagome weave patterns for the fabrication of interlaced lattice structures using straight strips*, in: *Advances in Architectural Geometry 2018*, Chalmers University of Technology, 2018, pp. 72–93.
- [24] P. Ayres, S. Bornaz, A. Orlinski, M. Heimrath, A. G. Martin, *Architectural scale kagome weaving: Design methods and fabrication concepts*, in: *FABRICATE: Design & Making*, UCL Press, 2020, pp. 178–185.
- [25] Y. Ren, J. Panetta, T. Chen, F. Isvoranu, S. Poincloux, C. Brandt, A. Martin, M. Pauly, *3d weaving with curved ribbons*, *ACM Transactions on Graphics (TOG)* 40 (4) (2021) 1–15.
- [26] C. Baek, A. G. Martin, S. Poincloux, T. Chen, P. M. Reis, *Smooth triaxial weaving with naturally curved ribbons*, *Physical Review Letters* 127 (10) (2021) 104301.
- [27] E. Soriano, R. Sastre, D. Boixader, *G-shells: Flat collapsible geodesic mechanisms for gridshells*, in: *Proceedings of IASS Annual Symposia*, Vol. 2019, International Association for Shell and Spatial Structures (IASS), 2019, pp. 1–8.
- [28] S. Pillwein, K. Leimer, M. Birsak, P. Musialski, *On Elastic Geodesic Grids and Their Planar to Spatial Deployment*, *ACM Transactions on Graphics* 39 (4) (2020) 12.
- [29] S. Pillwein, J. Kübert, F. Rist, P. Musialski, *Design and fabrication of elastic geodesic grid structures*, *SCF '20: Proceedings of the ACM Symposium on Computational Fabric ation* (2020) 11.
- [30] J. Panetta, M. Konaković-Luković, F. Isvoranu, E. Bouleau, M. Pauly, *X-shells: A new class of deployable beam structures*, *ACM Transactions on Graphics (TOG)* 38 (4) (2019) 1–15.
- [31] C. Tang, M. Kilian, P. Bo, J. Wallner, H. Pottmann, *Analysis and design of curved support structures*, in: S. Adriaenssens, F. Gramazio, M. Kohler, A. Menges, M. Pauly (Eds.), *Advances in Architectural Geometry 2016*, VDF Hochschulverlag, ETH Zürich, 2016, pp. 8 – 23.
- [32] E. Schling, M. Kilian, H. Wang, D. Schikore, H. Pottmann, *Design and construction of curved support structures with repetitive parameters*, in: L. H. et al. (Ed.), *Adv. in Architectural Geometry*, Klein Publ. Ltd, 2018, pp. 140–165.
- [33] D. Pellis, H. Wang, M. Kilian, F. Rist, H. Pottmann, C. Müller, *Principal symmetric meshes*, *ACM Trans. Graphics* 39 (4) (2020) 127:1–127:17.

- [34] M. R. Jimenez, C. Müller, H. Pottmann, Discretizations of surfaces with constant ratio of principal curvatures, *Discrete and Computational Geometry* 63 (2020) 670–704.
- [35] H. Wang, H. Pottmann, Characteristic parameterizations of surfaces with a constant ratio of principal curvatures, *Computer Aided Geometric Design* 93 (2022) 102074.
- [36] Y. Liu, H. Pottmann, J. Wallner, Y.-L. Yang, W. Wang, Geometric modeling with conical meshes and developable surfaces, *ACM Trans. Graphics* 25 (3) (2006) 681–689.
- [37] H. Pottmann, J. Wallner, The focal geometry of circular and conical meshes, *Advances in Computational Mathematics* 29 (3) (2008) 249–268.
- [38] F. Wenzel, B. Frese, R. Barthel, Die Holzrippenschale in bad dürkheim, *Bauen mit Holz* (1987) S–282.
- [39] J. Natterer, N. Burger, A. Müller, J. Natterer, Holzrippendächer in brettstapelbauweise-raumerlebnis durch filigrane tragwerke, *Bautechnik* 77 (11) (2000) 783–792.
- [40] J. Chilton, G. Tang, *Timber gridshells: architecture, structure and craft*, Routledge, 2016.
- [41] E. Soriano, Low-tech geodesic gridshell: Almond pavilion, *ArchiDOCT* 4 (2) (2017) 29–38.
- [42] C. Haskell, N. Montagne, C. Douthe, O. Baverel, C. Fivet, Generation of elastic geodesic gridshells with anisotropic cross sections, *International Journal of Space Structures* 36 (4) (2021) 294–306.
- [43] E. Schling, D. Hitrec, J. Schikore, R. Barthel, Design and construction of the asymptotic pavilion, in: K.-U. Bletzinger, E. Oñate, B. Kröplin (Eds.), *VIII International Conference on Textile Composites and Inflatable Structures*, International Center for Numerical Methods in Engineering (CIMNE), 2017, pp. 178–189.
- [44] T. Oberbichler, Bowerbird, <http://github.com/oberbichler/Bowerbird>.
- [45] T. Oberbichler, E. Schling, Tracing curvature paths on trimmed multipatch surfaces, submitted to *Computer Methods in Applied Mechanics and Engineering*.
- [46] E. Schling, Z. Wan, A geometry-based design approach and structural behaviour for an asymptotic curtain wall system, *Journal of Building Engineering* (2022) 104432.
- [47] J. Schikore, E. Schling, T. Oberbichler, A. M. Bauer, Kinetics and design of semi-compliant grid mechanisms, *Adv. Archit. Geom* (2021) 108–129.
- [48] M. do Carmo, *Differential Geometry of Curves and Surfaces*, Prentice-Hall, 1976.
- [49] W. Kühnel, *Differential geometry*, Vol. 77 of *Student Mathematical Library*, American Mathematical Society, Providence, RI, 2015.
- [50] W. K. Schief, A. I. Bobenko, T. Hoffmann, On the integrability of infinitesimal and finite deformations of polyhedral surfaces, in: *Discrete differential geometry*, Springer, 2008, pp. 67–93.
- [51] N. Montagne, C. Douthe, X. Tellier, C. Fivet, O. Baverel, Voss surfaces: A design space for geodesic gridshells, *Journal of the IASS* 61 (4) (2020) 255–263.
- [52] C. Tang, X. Sun, A. Gomes, J. Wallner, H. Pottmann, Form-finding with polyhedral meshes made simple, *ACM Trans. Graph.* 33 (4) (2014) 70:1–70:9.
- [53] H. Pottmann, M. Hofer, Geometry of the squared distance function to curves and surfaces, in: H.-C. Hege, K. Polthier (Eds.), *Visualization and Mathematics III*, Springer, 2003, pp. 223–244.
- [54] A. Jacobson, D. Panozzo, et al., libigl: A simple C++ geometry processing library, <https://libigl.github.io/> (2018).
- [55] D. Bommers, H. Zimmer, L. Kobbelt, Mixed-integer quadrangulation, *ACM Transactions On Graphics (TOG)* 28 (3) (2009) 1–10.
- [56] G. Farin, *Curves and surfaces for CAGD*, Morgan Kaufmann, 2002.
- [57] B. Steve, D. Scott, P. Andy, The hops component, <https://developer.rhino3d.com/guides/compute/hops-component/> (2021).